Stress-Induced Changes in Glutamate Release and Turnover:

A PET [^{11}C]ABP688 & MRS Study

Marie Sato Fitoussi, B.Sc.

Integrated Program in Neuroscience

McGill University, Montreal

Submitted April 2020

A thesis submitted to McGill University in partial fulfillment of the requirements of the degree of Master of Science

© Marie Sato Fitoussi 2020

TABLE OF CONTENTS

LIST OF ABBREVIATIONS

ABP688	3-(6-methyl-pyridin-2-ylethynyl)-cyclohex-2-enone oxime
ACC	Anterior cingulate cortex
AMPA	α-amino-3-hydroxy-5-methyl-4-isoxazolepropionic acid
BBB	Blood brain barrier
BP_{ND}	Binding potential, non-displaceable
dlPFC	Dorsolateral prefrontal cortex
DSM-IV	Diagnostic and Statistical Manual of Mental Disorders, fourth edition
DVR	Distribution volume ratio
EAAT	Excitatory amino acid transporter
FPEB	3-fluoro-5-[(pyridin-3-yl)ethynyl]benzonitrile
GABA	γ-aminobutyric acid
Gln	Tissue concentration of glutamine
Glu	Tissue concentration of glutamate
Glx	Tissue concentration of glutamate + glutamine
HPA	Hypothalamo-Pituitary Adrenal
HPLC	High performance liquid chromatography
HRRT	High resolution research tomograph
iGluR	Ionotropic glutamate receptor
LTD	Long-term depression
LTP	Long-term potentiation
MDD	Major Depressive Disorder
mGlu(1-5)	Metabotropic glutamate receptor
MPEP	6-methyl-2-(phenylethynyl)pyridine
mPFC	Medial prefrontal cortex
MRI	Magnetic resonance imaging
MRS	Magnetic resonance spectroscopy
NAM	Negative allosteric modulator

NMDA	*N*-methyl-*d*-aspartate
OFC	Orbitofrontal cortex
PAM	Positive allosteric modulator
PFC	Prefrontal cortex
PET	Positron emission tomography
PTSD	Post traumatic stress disorder
ROI	Region of interest
SRTM	Simplified reference tissue model
VAS	Visual analog scale
V_{ND}	Non-displaceable volume of distribution
V_T	Total volume of distribution

ACKNOWLEDGEMENTS

I wish to express my gratitude to my late supervisor Dr. Chawki Benkelfat for giving me the opportunity to learn from him despite his illness and for his attentive mentorship. I am also eternally grateful to Dr. Marco Leyton, who took over the role of supervision in the writing phase of this work. The completion of this degree would not have been possible without his generous and patient guidance. The contribution of former lab members Dr. Atsuko Nagano-Saito and Dr. Kelly Smart who designed and helped to initiate the project has also been critical to this project.

All the members of the lab were also supportive throughout my degree. I especially wish to wholeheartedly thank the lab nurse Dominique Allard for her dedicated assistance with subjects screening. My time at the was often a humbling as I was surrounded by my colleagues and friends Hussein and Maisha, as well as Dr. Gobbi lab trainees, who have shown support and encouragement throughout numerous conversations.

Further, I would like to thank my advisory committee members for their helpful advice and honest critiques. I am also very grateful to my mentor for her invaluable support and troubleshooting.

These projects were made possible by the work of many collaborators, including the members of the Translational Neuroimaging Laboratory. In particular, I am deeply thankful to Dr. Pedro Rosa-Neto, who has allowed me to unofficially join their lab and who has shown passionate enthusiasm for my work and brought up perspectives on the projects while maintaining an extremely demanding schedule. I also thank Peter Kang for teaching me various neuroimaging analysis skills and Joseph Thierrault to whom I frequently turned to with questions. I wish to acknowledge the work of the imaging staff at the McConnell Brain Imaging Centre, including PET Unit, the cyclotron team, and the MRI technologists. A special thanks to Reda Bouhachi and Chris Hsiao who made scanning an enjoyable time.

Finally, I would like to thank all the healthy volunteers who participated in this research.

CONTRIBUTION OF AUTHORS

Ethics and funding: Dr. Chawki Benkelfat and Dr. Kelly Smart

Study design: Marie Sato-Fitoussi, Dr. Chawki Benkelfat, Dr. Kelly Smart and Dr. Atsuko Nagano-Saito

Data collection: Marie Sato-Fitoussi

Data analysis: Marie Sato- Fitoussi, Peter Kang, and Dr. Atsuko Nagano-Saito

Preparation of the thesis: Marie Sato-Fitoussi and Dr. Marco Leyton

ABSTRACT

Abnormal glutamate transmission is implicated in stress-related psychiatric disorders. Our ability to study the transmitter's role in disease states and responses to therapeutic interventions would be greatly improved by the availability of a non-invasive method for the in vivo quantification of human brain glutamate release. One option is positron emission tomography (PET) with the labeled tracer, [$_{11}$C]ABP688. ABP688 is a highly selective antagonist that binds to an allosteric site of the type 5 metabotropic glutamate receptor. Pharmacological challenge studies have raised the possibility that it might be responsive to acute glutamate fluctuations. Here, we explored [$_{11}$C]ABP688's sensitivity to a laboratory stressor, an environmental manipulation known to induce glutamate release in research animals, as measured with microdialysis, and increase glutamate turnover in humans, as measured with magnetic resonance spectroscopy (MRS). Control and stress PET and MRS sessions were acquired at least three days apart, in a randomized, counter-balanced order, in nine healthy volunteers (5 M, 4 F). Mood and physiological parameters were measured throughout. An effect of the stressor was confirmed by significant changes in self-reported mood ($ps < 0.041$), sympathetic system activations ($ps < 0.042$), and the MRS index of striatal glutamate reuptake following excitatory neurotransmission, Glx/Cr levels ($p = 0.048$). These effects were not accompanied by significant changes in [$_{11}$C]ABP688 BP_{ND} ($ps > 0.21$), but BP_{ND} values on the stress session were negatively correlated with stress-induced changes in cortisol AUC ($ps < 0.044$) and the Glx:Glu ratio in the ACC ($ps < 0.045$). Together, these findings suggest that [$_{11}$C]ABP688 is not suitable for measuring moderate fluctuations in extra-cellular glutamate even though [$_{11}$C]ABP688 BP_{ND} and the MRS quantification of glutamate turnover might not be fully independent of each other.

RÉSUMÉ

La transmission altérée du glutamate est impliquée dans de nombreuses maladies psychiatriques liées au stress. Notre capacité à étudier le rôle du neurotransmetteur dans les états pathologiques ainsi qu'en réponse aux interventions thérapeutiques serait grandement amélioré si une méthode non-invasive permettant de quantifier in vivo la libération de glutamate endogène serait disponible, une option étant la tomographie par émission de positrons (TEP) avec le radiotraceur [$_{11}$C]ABP688. [$_{11}$C]ABP688 est un antagoniste hautement sélectif qui se lie au niveau du site allostérique du récepteur métabotropique du glutamate de type 5. Des études moyennant l'administration de drogues provoquant des variations au niveau de la transmission du glutamate ont suggérées la possibilité que ce ligand pourrait être réactif aux fluctuations aigues du glutamate quantifiées par micro-dialyse. Ici, nous explorons la sensibilité de [$_{11}$C]ABP688 à un protocole de stress, faisant partie des manipulations environnementales connu pour induire la transmission de glutamate chez les animaux de laboratoire, telle que mesurée par micro-dialyse, et des changements dans le renouvellement du glutamate chez les humains mesurés par spectroscopie RMN. Des sessions controles et de stress de TEP et de spectroscopie RMN ont été obtenu chez neuf volontaires sains (5M et 4F), avec au moins trois jours d'intervalle, dans un ordre randomisé et contrebalancé. Les paramètres psychologiques et physiologiques ont été mesurés durant les sessions. Un effet du stimulus a été confirmé par une variation significative des mesures auto-déclarées de l' humeur ($ps < 0.041$), l'activation du système nerveux sympathique ($ps < 0.042$vii) et par un index spectroscopique de recaptage de glutamate suivant sa libération présynaptique dans le striatum ($p = 0.048$). Ces effets n'ont pas été accompagnés par un changement significatif du potentiel de liaison de [$_{11}$C]ABP688 ($ps > 0.21$), mais le potentiel de liaison durant la session de stress était négativement corrélé avec la variation d'ASC du cortisol ($ps < 0.045$), et avec la variation du ratio Glx:Glu dans le CCA ($ps < 0.044$). De façon préalable, nous avons donc établi que les quantifications du potentiel de liaison de [$_{11}$C]ABP688 et du renouvellement de glutamate ne semblent pas être deux mesures totalement indépendantes l' une de l' autre. Il n'en reste pas moins que le ligand [$_{11}$C]ABP688 ne serait pas apte à capter des fluctuations modérées de glutamate extra-cellulaire.

INTRODUCTION

1.1 Overview

1.1.1 Stress

To survive, humans and other animals need the ability to promptly meet demands imposed by a wide range of challenges. The brain guides these coping responses, both behavioral and physiological (1), and together they compose situation-appropriate "fight-or-flight." In the short-term, these responses are protective and enhanced by activations of the Hypothalamic-Pituitary-Adrenal (HPA) axis, the autonomic nervous system, and the immune system. In addition to constituting the immediate adaptations, they also promote learning and memory functions that allow organisms to respond more effectively to future threats (2). If, however, these processes are engaged when they should not be, or if they remain activated for prolonged periods, they can become maladaptive (3).

1.1.2 Stress-induced psychiatric disorders

The inability to cope with a threat is a major risk factor affecting the onset, symptom expression, and relapse of several neuropsychiatric disorders, including mood disorders and post-traumatic stress disorder (PTSD) (4). There is evidence that PTSD and episodes of mania can be triggered by exposure to a single traumatic event (5) In comparison, a combination of both chronic and acute stress appears to be most relevant for addictions and major depressive disorder (MDD) (6).

Stressful events are thought to affect these disorders by inducing long-lasting neuroplastic changes (1,7). As such, studying the long-term consequences of acute stress can provide insight into the underlying neurobiology (8). For example, overexposure to glucocorticoids in the hippocampus is associated with dendritic atrophy and loss of dendritic spines, suppression of neurogenesis and neuronal death in pyramidal cells, fitting with the loss of hippocampal volume seen in animal

models of depression (9). Interestingly, neuronal growth is seen in the amygdala, which is a key region for the mediation of fear responses (10). Other vulnerable regions to stress include the prefrontal cortex (7). Like the hippocampus, it contributes to learning and memory, potentially accounting for the development of stress-related cognitive dysfunctions (11).

1.2 Brain glutamate: relevance to stress

1.2.1 Glutamate signaling

Glutamate is the most abundant neurotransmitter in the central nervous system (CNS), present in more than half of all brain synapses. Following its synthesis from glutamine in the synaptic nerve terminal, glutamate is packed into synaptic vesicles via transporters (12), ready for synaptic release. The high concentrations of intracellular glutamate require tight regulatory processes (13) to limit extracellular levels and to ensure optimal neurotransmission. Non-neuronal cells play a major role in this respect. Following release into the synaptic cleft, the large majority of clearance is mediated by a family of excitatory amino acid transporters (EAATs, subtypes 1-5) that transport glutamate into astrocytes. Astrocytic glutamate is then converted to glutamine by the enzyme, glutamate synthetase. Glutamine is transported back to glutamatergic neurons and resynthesized to glutamate when additional quantities of glutamate are required.

Glutamate can induce both fast synaptic signalling and slow, modulatory effects. The fast signalling effects are mediated through three ionotropic (iGlu) receptors, N-methyl-D-aspartate (NMDA), a-amino-3-hydroxy-5-methyl-4-isoazolepropionic acid (AMPA) and kainic acid (KA) receptors (14). The slow, modulatory actions are mediated by metabotropic receptors (15,16). These mGlu binding sites constitute a family of eight class G-protein-coupled receptors (mGlu1-8) that are divided into three groups based on sequence homology, ligand binding, and G-protein coupling specificity (17). Activation of mGlu receptors can promote neuroplastic changes through

engagement of second messenger signaling mechanisms (18).

1.2.2 Structure, Function, and Regional Expression of mGlu5

mGlu5 receptors are part of the Group I mGlu receptor family, comprising mGlu1 and mGlu5. When stimulated, both of these receptors activate the phospholipase C pathway via Gq signaling (19). The mGlu5 receptors possess a large bi-lobed N-terminal domain, separated from the seven transmembrane regions by a cysteine-rich region and agonist binding to the cavity, bringing the lobes closer to one another. This so-called Venus flytrap receptor activation induces a conformation change to the binding site that gets closer to the transmembrane domain (20). Glutamate binding also triggers the switch to a dimeric state, with a disulfide bridge binding two activated receptors (21).

mGlu5 receptors are primarily located in the periphery of the postsynaptic terminal (22) but also on glial cells (23,24). Moreover, although mGlu5 is distributed throughout the brain, immunohistochemical studies in the rat show highest density in limbic regions and the neocortex, moderate levels in the striatum and thalamus, and lower expression in the cerebellum (25,26).

1.2.3 The glutamate system in the acute stress response

Acute stress can induce both rapid and prolonged changes in synaptic function involving modulation of glutamate neurotransmission (27). Studies in laboratory animals identify a central role in glucocorticoids, which elicit glutamate release (28–30) in regions associated with memory, learning and affect, such as the prefrontal cortex (PFC) (27,30). Ample evidence implicates both genomic and non-genomic pathways (3) in several control points of the tripartite synapse (reviewed by Popoli et al., (31)), including glutamate release (28) and glutamate receptor

trafficking with the activation of NMDA receptors (23). Glucocorticoids also play a role at a non-neuronal level, reducing the number of glial cells, and thus glutamate clearance.

Acute stress-induced increases in corticosterone reduce the expression of mGlu5 receptors in laboratory animals (28). Although human studies investigating stress-induced glutamate changes are scarce, preliminary evidence suggests that similar effects are occurring. Proton magnetic resonance spectroscopic (MRS) analyses have found evidence of increased cortical glutamate and glutamine levels during acute painful stimulation in humans (32,33), consistent with enhanced glutamate cycling following exposure to an uncontrollable aversive stimulus. This pain-related change in glutamate metabolism can be reduced by a perceived capacity to control the adverse event, indicating that the response is influenced by the cognitive appraisal of the stimulus, not just the stimulus intensity (34). Chemically induced panic was also reported to increase glutamate levels (35) but a study benefiting from high magnetic field strength (7T) failed to demonstrate changes in glutamate levels following psychosocial stress (36).

1.2.4 Glutamate in stress-related disorders

Adequate functioning of the glutamatergic system is crucial for maintaining mental health. While the dopamine system has long been a research target in stress-related psychopathologies, glutamate abnormalities are increasingly considered to be a core feature in these disorders.

In animal models of depression, hyperactivity of the glutamatergic system is commonly seen, potentially leading to excitotoxicity and impaired synaptic integrity, thereby contributing to the observed brain abnormalities. In people with mood disorders, there is also in vivo evidence of lower mGlu5 receptor expression, though this has been seen in some studies (37) but not others (38). There is evidence that these effects are brain region specific, with reports of decreased

glutamate in the anterior cingulate cortex (39) and increases in the occipital cortex (40). Overall, though, there appears to be a pattern of reduced glutamine to glutamate ratios, possibly reflecting reduced glutamate conversion to glutamine (41).

Over the past decade, evidence has accumulated that pharmacological manipulations of glutamate can provide a novel mechanism for the treatment of mood disorders. To date, ketamine is the most successful glutamatergic treatment, showing rapid antidepressant effects after a single dose (42). Through the antagonism of NMDA receptors, it induces a rapid and transient surge in glutamate. Subsequent post-synaptic AMPA receptor activation is thought to then initiate a signaling pathway cascade that promotes neuroplasticity and the antidepressant effect (43).

In some, though not all studies, mGlu5 binding availability is decreased following ketamine administration (44,45). This effect was unexpected given the tentative evidence that mGlu5 is reduced in MD (45). Alterations to mGlu5 receptors have also been implicated in PTSD (46). A neuroimaging study identified elevated mGlu5 receptor expression in people with PTSD, possibly underlying the upregulation of SHANK-1 gene expression observed in post-mortem brain tissue (46).

Studies in laboratory animals raise the possibility that, for both disorders, altered mGlu1- and mGlu5 transmission can disrupt long-term depression (LTD) and long-term potentiation (LTP). These mGlu effects might be promoted by stress-induced glucocorticoid release, and alter the ability to both form and extinguish fear conditioning (47), thereby disrupting emotion-related fear learning and resilience to traumatic memory-associated anxiety (11).

1.3 Studying glutamate neurotransmission in humans: [$_{11}$C]ABP688 and MRS

The development of molecular neuroimaging techniques has revolutionized the ability to non-invasively gain insight into the organization of living human brain.

1.3.1 The basic principles of PET

Positron emission tomography (PET) provides a relatively non-invasive tool to explore neurotransmitter systems that are hypothesized to be altered in psychiatric disorders (48). A state-of-the-art, brain dedicated High-Resolution Research Tomograph (HRRT) provides spatial resolution of up to 2.2 mm (49), permitting reliable quantification of different physiological functions in brain structures including in small brain nuclei. This technique relies on the injection of low doses of radioactively labeled tracers (ligand) that interact with the targeted biological system. The amount of the processed signal mirrors the relative activity of the targeted biochemical process.

The radioligands are created by incorporating an unstable isotope into a carrier molecule (precursor). The neutron deficient compound will reach a stable state by undergoing radioactive decay, during which positrons will be emitted. In the case of carbon-11 ($_{11}$C) labeled radiotracers, the physical half-life is short (20min), so that injection should immediately follow its production in the cyclotron (50).

For a tracer to be a successful imaging probe for PET, it must fulfill several criteria that mainly stem from the need to increase the signal-to-noise ratio; i.e., avoiding radioactivity in non-target sites. Hydrophobicity of the tracer is critical since the tracer must diffuse through the blood-brain barrier (BBB). Moreover, a suitable tracer for receptor imaging should exhibit high affinity for the target of interest. The binding should be selective to the target of interest, thereby limiting tracer

accumulation in regions with low target expression, and the tracer must clear rapidly from these sites. The binding should also be faster than isotope decay and should allow for short acquisition time. Finally, the tracer should be metabolically stable for the duration of the acquisition, as isotope dissociation from the molecular precursor will result in the imaging of the free isotope or the metabolites instead of the labeled tracer (51,52).

1.3.2 Annihilation coincidence

Once expelled from the nucleus, a positron travels a short distance before colliding with an electron in the surrounding tissues. This phenomenon, referred to as annihilation, results in the production of gamma rays made up of two high-energy photons (511 KeV) that are simultaneously released at nearly opposite direction ($180^{o}\pm0.25^{o}$). The energy of these photons is sufficient to allow most of them to pass through the subject body (53). If these two photons are detected within a certain time of each other (coincidence time window, less than 2-3 nanoseconds) it is then assumed that they both originated from the same annihilation process of a given positron emitted during decay and will launch a coincidence circuit. The location and direction of any coincidence at a given time is unique, so that the positron is emitted somewhere between the line created by the two photons. A PET scanner consists of a circular array of detectors that form a ring of scintillation crystal and each detector can form a coincidence line with any one of the opposing detectors, such that a series of parallel coincidences are formed. Images acquired by the scanner are therefore a collection of these events that allows gathering positional information of the positron emitter. The particulars are stored in two-dimensional matrices called sinograms. The raw data are then reconstructed into cross-sectional tomographic images (53).

1.3.3 Attenuation correction and PET/MR co-registration

In addition to the tracer kinetic requirements mentioned above, features of the isotope and scanner also affect PET image quality and detection sensitivity. Most importantly, PET detects the annihilation point. The lower the energy of the isotope, the shorter the distance that the radiotracer travels before annihilating, and thus the higher is the resolution. The energy of ^{11}C labeled tracers equates to ~ 0.3-0.4 mm (54). The possibility that two annihilations from a different point of decay occur at a very short interval of time cannot be excluded, thereby launching a coincidence circuit between two distinct events and leading to mispositioning of the point. Similarly, detection of true coincidence counts can also be lost by interaction and subsequent absorption of energy by dense molecules of brain tissues or random scattering of photons outside the field of view of the detector. This results in an increase in image noise, artifacts and distortion, which would prevent accurate quantification of PET tracer activity. In order to address the above, attenuation correction of the emission data is required. This consist of the use of an external radiation source before or after acquisition of emission to obtain a transmission image showing an attenuation map of the subject brain tissues. This correction still does not compensate for the major drawback from which PET suffers owing to the relatively low spatial resolution, that is the lack of anatomical information. On the other hand, high-resolution structural images can be obtained with Magnetic Resonance Imaging (MRI) and can serve as an anatomical orientation guide for PET information. Thus, same-subject co-registration of PET and MRI can circumvent weakness of modalities by combining accurate anatomical and functional information from the same subject (55).

1.3.4 The simplified reference tissue model for estimating PET tracer binding

The use of an arterial line to generate blood sample derived input functions is the gold standard for yielding absolute measures from dynamic PET data. However, the insertion and removal of

arterial lines can be uncomfortable. This invasive technique can be avoided for some tracers when there exists a brain region where the tracer would not accumulate because it is devoid of the target of interest. In these cases, the time course of the tracer uptake in the tissue of interest is expressed relative to its uptake in the tissue without target specific binding sites (56). In addition to the absence of specific binding, it is important that volume of distribution of the non-specific binding is identical for both tissues. Under these conditions, binding parameters, relative to the comparison region can be calculated by using a two-tissue compartment model for the target region. Since a reference region is devoid of specific binding, the exchange between non-displaceable (free and non-specific) and specific binding is fast enough, allowing the model to be further simplified and described by a single tissue compartment. The outcome measure obtained is binding potential, non-displaceable (BP_{ND}), which refers to the ratio at equilibrium of specifically bound radioligand to that of non-displaceable radioligand in the tissue (57) and is equivalent to the ratio of the kinetic constants k_3 over k_4 (k_3/k_4) in the two-tissue compartment model (58). BP_{ND} values simultaneously reflect the availability and affinity of receptor binding sites for its tracer because it is directly proportional to the autoradiography single-dose experiment in vitro measures of B_{max} (concentration of available binding sites) and 1/Kd (inverse of dissociation constant, i.e. affinity) (59).

1.3.5 [^{11}C]ABP688

mGlu5 PET radioligands such as ^{11}C-M-MPEP and ^{11}C-M-FPEP are conformational glutamate analogs that competitively interact at the N-terminal orthostatic binding site that also binds glutamate (60,61). However, these ligands are not suitable PET tracers since they lack subtype selectivity and have either low binding affinity or high lipophilicity or metabolism, yielding unfavorable brain uptake kinetics (60–63). In contrast, current mGlu5 PET ligands are allosteric

modulators, which occupy the cell transmembrane domain of the receptor rather than the orthosteric binding site. They are more suitable as PET probes because they have greater subtype selectivity due to the putative heterogeneity of allosteric sites. In this respect, the ligand 3-(6-methyl-pyridin-2-ylethynyl)cyclohex-2-enone-O-11C-methyloxime ([^{11}C]ABP688) shows fast and favorable kinetics: it binds with high selectivity but also exhibits high affinity to mGlu5 receptors (64) with a dissociation constant of K_d = 5.7 nM, as determined by Kawamura et al. (65). Moreover, it shows good blood–brain barrier permeability (extraction fraction > 0.9, Wyss et ml., 2007 (66)) due to its optimal lipophilicity (logP = 2.4, (63)) as well as hydrophilic metabolites that are non-brain permeable. This promising radiopharmaceutical occupation induces conformation changes in the receptor, followed by reduction of glutamate binding (63) and is displaceable by 2-methyl-6-(phenylethynyl)-pyridine (MPEP), another allosteric modulator from which it is derived. Therefore, it is considered to be a negative allosteric modulator.

[^{11}C]ABP688 binding is very sensitive to isomer content due to higher affinity for the receptor of the (E) isomer. Even modest levels of Z content (less than 10%) have been shown to influence BP_{ND} values (65,67). Our lab recently developed a High-Performance Liquid Chromatography (HPLC) purification method (68) to reliably produce diastereomerically pure (E) - [^{11}C]ABP688 isomer with high chemical and radiochemical purity, notwithstanding the precursor isomeric enrichment, allowing consistent and accurate calculations.

The simplified reference tissue model derivation of non-specific binding in cerebellar grey matter (28) can be used for deriving specific-to-non-specific [^{11}C]ABP688 BP_{ND} values. Use of the cerebellum as a reference region is based on *in vivo* and *in vitro* evidence that tracer uptake is extremely low in the cerebellum compared with other regions (63,69), despite no clear evidence of a region fully devoid of $mGlu_5$ receptors (66,70,71). In support, blockade study with a mGlu5

receptor antagonist does not seem to affect binding in the cerebellum (72). Most importantly, studies in both humans and laboratory animals demonstrate a high correspondence (r=0.97) between BP_{ND} values and k3/k4 kinetics constants ratio estimates calculated using the arterial input function (59,69).

1.3.5.1 Evidence that [^{11}C]ABP688 BPND values reflect brain regional mGlu5 receptor levels

Several lines of evidence have established that PET imaging with [^{11}C]ABP688 is a promising tool to map mGlu5 receptor availability throughout the brain, although receptor availability may not be directly linked to function. In vitro studies show that the tracer binds to mGlu5 at the plasma membrane but is not sufficiently cell membrane permeable to penetrate and bind to internalized receptors (38). Hence, it appears to solely target mGlu5 accessible on the cell surface in vivo, allowing to gain insight into changes in receptor availability associated with psychiatric diseases (73–75). The largest alteration in [^{11}C]ABP688 mGlu5 binding was found in people addicted to tobacco cigarettes (76). These reductions in mGlu5 binding availability are related to the tobacco use since mGlu5 binding normalizes following long-term smoking abstinence (75).

In laboratory animals, the highest brain regional [^{11}C]ABP688 uptake is observed in the striatum, cortex, and hippocampus, corresponding to mGlu5 receptor dense regions (25) as measured in post-mortem brain tissue from rats (63,69). These studies also demonstrate negligible binding in the cerebellum and white matter where mGlu5 expression is minimal. Similarly, in vivo studies in humans show heterogeneous accumulation patterns of the tracer that reflects known mGlu5 receptor distribution throughout the brain (66,77). Moreover, a group comparisons PET study revealed reductions in mGlu5 receptor binding in subjects with MDD (37), although some groups did not find any differences (38,78). These alterations were in line with reductions in receptor

density demonstrated in post-mortem assessment (37), suggesting that ^{11}C-ABP688 binding may reflect mGlu5 receptor protein expression.

1.3.5.2 Evidence that changes in [^{11}C]ABP688 BPND reflect changes in extracellular glutamate

Available binding site to mGlu5 receptor allosteric site depends on the tertiary and quaternary conformation of the receptor, which in turn is largely influenced by glutamate level and binding to the Venus flytrap domain as mentioned above (Section 1.2.2). Thus, [^{11}C]ABP688 binding may be sensitive to changes in the affinity of the allosteric site induced by extracellular glutamate fluctuations (44).

This is supported by recent pharmacological challenges in laboratory animals (79–81). Of interest, a microdialysis and PET study in rats found decreased extracellular glutamate levels combined with increased [^{11}C]ABP688 binding following administration of ceftriaxone, an activator of the glutamate transporter GLT-1. The same mechanism may underlie the finding of consistent increase in [^{11}C]ABP688 binding upon repeated same-day test-retest study in a group of human controls. The authors suggested that the participants experienced decreased anxiety during the follow-up scan, leading to diminished stress-induced glutamate release (82). The observed pattern is in line with preclinical evidence for diurnal variations in glutamate levels (83). It has been specifically shown that glutamate level is increased during dark cycle and decreased during light cycle, possibly consistent with quantification of lower receptor availability in the morning scan. A recent study with [^{11}C]ABP688 in rodents also showed circadian variation in mGlu5 receptor binding further supporting this interpretation (84).

The sensitivity of [^{11}C]ABP688 binding to pharmacologically induced glutamate variation has also been tested in human. Ketamine, an NMDA receptor antagonist known to promote glutamate release, led to widespread decreases in [^{11}C]ABP688 binding in humans (44,45). Receptor internalization has previously been described in the context of dopaminergic neurotransmission, where persisting decrease in binding of D2 receptors radioligand [^{11}C]raclopride was observed following dopamine release (85). Thus, the long-lasting reduction in [^{11}C]ABP688 binding of up to 24h observed here could be explained by a glutamate surge-induced decrease in membrane mGlu5 receptor expression.

These studies highlight the wide range of possible mechanisms by which varying levels of glutamate may be affecting [^{11}C]ABP688 binding to mGlu5 receptors, including receptor internalization, functional state of the receptor or the total amount of protein in the cell surface membrane (44,80). Even so, a direct relationship between changes in the tracer binding and extra-cellular glutamate levels has not been verified. Although a correlation between [^{11}C]ABP688 values and MRS measured glutamate levels were obtained in a study testing MDD subjects (38), this was not replicated in cocaine-dependent men and healthy volunteers (74). In addition, high variability has still been described in assessing test-retest reliability with consistent scanning conditions, tentatively eliminating known possibilities for variations in glutamate release (86).

Taken together, the influence of glutamate release on [^{11}C]ABP688 quantification in humans remains speculative and poorly understood. Psychological factors such as situational anxiety or stress could be relevant to the hypothesized influence of glutamate fluctuations on [^{11}C]ABP688 binding variability.

1.3.6 MRS

The scanning parameters used with MRI can be adapted to provide spectroscopic measures of some biochemical features in brain, in vivo. Compared to PET, proton magnetic resonance spectroscopy (^{1}H-MRS) is more favorable for repeated scan studies because it does not entail exposure to radioactivity. Moreover, at present, MRS is the only neuroimaging technique suitable for selectively measuring local glutamate (Glu) turnover rates in human brain. However, the method has a number of limitations. At 3T magnet strength, MRS can only detect compounds with a concentration of greater than 100M. This is suitable for measuring abundant neurotransmitters, such as glutamate (8–10 mmol/l) (87) and its metabolite, glutamine. Because glutamate and glutamine cortical concentrations are higher in the intracellular space, the MRS indices are thought to primarily reflect intracellular concentrations (41,87). This noted, the measures reflect a wide range of cellular populations (88) since anatomical resolution is approximately 7 to 40 mm^3.

While the majority of the brain glutamate is involved in cellular metabolism, the pool available for neurotransmission, which is later taken up by glial cells, is the major substrate for glutamine synthesis (89). Thus, static Glu measures could mask the detection of dynamic changes in synaptic glutamate and focus has been shifted towards the study of glutamine (Gln) that may better reflect neurotransmission (32,33). More specifically, the ratio of Gln over Glu (Gln:Glu) is potentially the most sensitive index to capture such changes, providing a window into the neuronal-glial coupling (41,90,91). In support, blockage of conversion in glial cells leads to Gln:Glu decrease, consistent with enrichment of glutamine in glial cells after glutamate release and relative presynaptic decrease of glutamate. Yet, care must be taken when assessing in vivo changes in Gln using MRS. Glu concentration can be sufficiently well resolved at magnetic fields of 2T and above due to the high separation of metabolites with coupled resonances (87,92). On the other hand, glutamine exhibits

a strongly coupled second-order spin system and its spectrum significantly overlaps with signals of similar chemical shifts including Glu and GABA (93,94) and it has been showed that accurate measurement of Gln requires higher magnetic strengths (>3T) (95,96). Hence, at the magnetic field strengths available in our site (3T), there can still be some ambiguity about spectral assignment with regards to Gln metabolites. For this reason, we analyzed and reported a combined fit of Glu and Gln, referred to as Glx (97,98).

1.4 Measures of Inflammation

Converging evidence suggests that inflammation could be a common pathway by which stress exposure increases risk for a wide range of disorders. Elevated markers of inflammation have been found in people with PTSD and mood disorders, including both MD and BD (99-101). The mechanism underlying these observations may be stress-induced dysregulations of the immune system, which can increase pro-inflammatory cytokines and decrease anti-inflammatory cytokines, especially when activation of these pathways is prolonged (102).

The importance of prolonged stress exposure is also suggested by the effects of GCs. Acute GC activation suppresses immune responses by at least two pathways, (i) the inhibition of the transcription factor NFκB major signaling pathway that mediates the transcription and translation of inflammatory mediators such as pro–IL-1β, IL-6, and TNF-α (103,104), and (ii) by enhancing expression of anti-inflammatory cytokines (105). In comparison, with chronic HPA axis activation, glucocorticoid resistance can develop, leading to excessive immune responses that could potentiate the development of psychiatric disorders.

Potentially aggravating these effects, recent research indicates that GCs also have pro-inflammatory impact on the immune system through pathways that are independent of NFκB activation by helping enzymatic cleavage of pro-inflammatory cytokines into their mature form. (106). Reports from different labs have confirmed increased levels of pro-inflammatory markers including interleukin 1 beta (IL- 1β), interleukin- 6 (IL- 6), and tumor necrosis factor- alpha (TNF- α) following administration of acute stressors (107,108) but also in tens of minutes following acute psychological stress (109). Given these observations, Il-1ß was measured in the current study as the immune response to stress with the most reliable signal.

1.5 Aims and Hypotheses

Aims

(1) To determine whether [$_{11}$C]ABP688 binding potential values measured with PET are affected by acute stress in healthy volunteers.

(2) To determine whether brain tissue glutamate and glutamine levels measured by MRS are affected by acute stress in healthy volunteers.

(3) To explore the relationships between [$_{11}$C]ABP688 BP_{ND} values and brain tissue glutamate and glutamine levels.

(4) To explore the relationship between [$_{11}$C]ABP688 BP_{ND} changes and psychological and physiological responses to stress exposure measured by self-report ratings, galvanic skin response, and stress-related hormones and cytokines.

Hypotheses

(1) A stressful stimulus administered to healthy volunteers immediately prior to a PET scan with [$_{11}$C]ABP688 will result in reduced BP_{ND} values, relative to a control scan.

(2) A stressful stimulus administered to healthy volunteers immediately prior to a MRS scan will result in increased Glx to Glu ratio, relative to a control scan.

(3) [$_{11}$C]ABP688 BP_{ND} value changes induced by acute stress will be negatively correlated with changes in MRS Glx to Glu ratio in the anterior cingulate cortex (ACC) and striatum.

(4) [$_{11}$C]ABP688 BP_{ND} changes will be significantly correlated with psychological and physiological responses to stress exposure.

MATERIALS AND METHODS

2.1 Participants

Healthy, right-handed volunteers aged between 20 and 40 years were recruited from the general population using online advertisements on the McGill University website and physical classifieds. Exclusion criteria included: (1) current or past DSM-5 disorders, including current or past substance use except for occasional cannabis use (< once per month), and social tobacco use (< once per week); (2) family history of DSM-IV Axis I disorder; (3) current or past chronic medication use, excluding birth control; (4) significant physical illness in the past 12 months; (5) any history of head injury or loss of consciousness; (6) any counter-indications to MRI or PET including claustrophobia, and the presence of a medical condition that makes pain stimuli dangerous (e.g., cardiac disease, hypertension, pulmonary disease, seizure disorder, osteopenia, and anxiety syndromes). The study protocol was approved by the Research Ethics Board of the Montreal Neurological Institute and the Faculty of Medicine and was carried out in accordance with the Declaration of Helsinki.

Following a preliminary telephone screen for major exclusion criteria, eligible volunteers were e-mailed more information about the study and invited to a full in-person screening using the Structured Clinical Interview for DSM-5 (SCID) (99) A urine toxicology test for illicit drugs of abuse (Triage, Biosite Diagnostics, San Diego, CA) and a urine pregnancy test for women was performed on the screening day and prior to each PET session. Next, physical health was evaluated by a routine examination by a medical doctor, standard blood work and an electrocardiogram. Participants who tentatively met the entry criteria underwent a final screening session to verify that they showed an adequate autonomic arousal response to the stressful stimuli. All participants were required to show an increase in skin conductance response of at least 10% immediately after

administration of the acute stress stimulus at the level of individual pain threshold (see section 2.1.2, Threshold determination).

2.1 Study design

Following screening and determination of stress threshold, all subjects underwent 4 scans on two separate days. Each session consisted of a 1-hour PET scan followed by a 45-min MRI scan with MRS. During "stress" session, participants underwent a 6-min stress task involving electrical stimulation to their wrist (see Stress administration section, described below) before each of the scans. This task was replaced by a resting period inside the scanner in the "rest" session, which served as a control. Thus, each participant served as their own control. See Figure 2 for a summary of the course of events. The two scanning days were conducted in a counter-balanced, within-subjects cross-over design, at least 3 days apart. The scans were conducted at the same time of the day.

2.1.1 Stress administration

The acute stress stimulus consisted of repeated unpredictable electric stimulation to the wrist administered immediately below the individual's pain threshold, which is the lowest intensity at which a sensation of mild pain is felt. Participants observed 20-second countdowns followed by a blank screen during which an electric stimulation occurred 67% of the time, pseudo-randomized. After a 10-second rest, the paradigm was repeated. In 6 minutes, participants had 12 x 30s blocks, for a total of 8 electrical stimulations out of 12 trials. Participants were instructed prior to the stress task that they would receive intermittent electrical stimulation at the level of their threshold. No distinguishing cue identified whether stimulation would be followed by a given countdown and participants were not informed of the contingency rate. Participants gave verbal ratings of

discomfort on the pain scale and visual analog scale (VAS; Fig. 1) every time the stimulus was presented, in order to adjust the intensity of the stimulus.

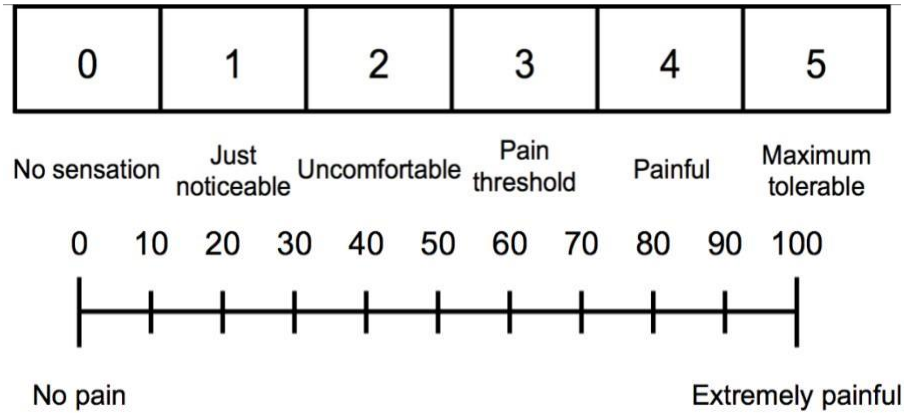

Figure 2.1: In order, pain scale and pain visual analog scale

.

2.1.2 Threshold determination

The stress response threshold was determined for each participant on a separate day, before their first imaging session and took place outside the PET scanner environment in order to avoid conditioned stress effects in the imaging environment. Electric stimulation was initiated with a duration of 200ms and voltage of 20V and was increased in increments of 2V until the lowest voltage at which subjects experienced moderate discomfort was reached. This was defined as a score of 3 on the 5-point pain scale and at least 20 on the VAS (Fig. 2.1). The threshold was re-established on the stress session, immediately prior to the stress task. The pain threshold determined earlier was used as a starting point in order to minimize the number of shocks administered before the task. The intensity of shock which corresponded to the threshold was then used as the target intensity for the stimulation during the stress task.

2.2 Objective indices of stress response

To assess the effectiveness of the stimuli, variation of the electrical conductance in response to skin secretion (electrodermal activity) was tracked continuously throughout stress/rest tasks and PET scanning sessions. First, phasic deflections in the skin conductance response (SCRs) were analyzed (100) . The amplitude of SCRs during stress task was calculated by subtracting the mean skin conductance level 2s before the expectation of a shock, from the peak value obtained immediately after administration of the shocks. In order to avoid habituation (101) , phasic increases occurring over the first 5 trials of shocks were taken into account. The same calculation was applied over the first 3 periods of blank screens in which shock was expected but not triggered. During the same time interval at rest, amplitudes of non-specific SCRs (occurring in the absence of stimuli) were calculated. Lastly, tonic skin conductance was also compared: 3 time intervals were averaged, including (1) stress task or rest, (2) the first 5 to 10 minutes of PET, and (3) the last 5 minutes of PET (Fig.2.2). The time interval (2) corresponds to the peak of the HPA axis response in response to stress, which is expected to begin 20 minutes after the initiation of the stimulus (t_2).

To measure the hypothalamus-pituitary-adrenal (HPA) axis cortisol response to stress, saliva samples were collected using oral swabs (Salimetrics, LLC). Six saliva samples were collected over 160 minutes, at baseline (t_1 and t_4) and at 2 time points after initiation of the task (t_2 and t_5: 20 min after initiation of the task, t_3 and t_6: end of the scans) while participants were in the scanner. Area under the curve with respect to ground (AUC_G) and with respect to increase (AUC_I) were calculated in each condition as described (102). AUC_G is the total area under the curve of all cortisol output, which takes into account the overall intensity at which cortisol responses were recorded, whereas the area between the ground and the first measure is ignored in AUC_I. Thus, AUC_I is

calculated with reference to the first value (cortisol value at t_1), emphasizing on whether any changes in cortisol response occurred over time. Il-1β values were also extracted from the 2 time points during the PET scan. (t_2 and t_3, as illustrated in Fig.2.2). Samples were stored at −20 °C until biochemical analysis took place. For three individuals, one to three samples were missing due to insufficient saliva.

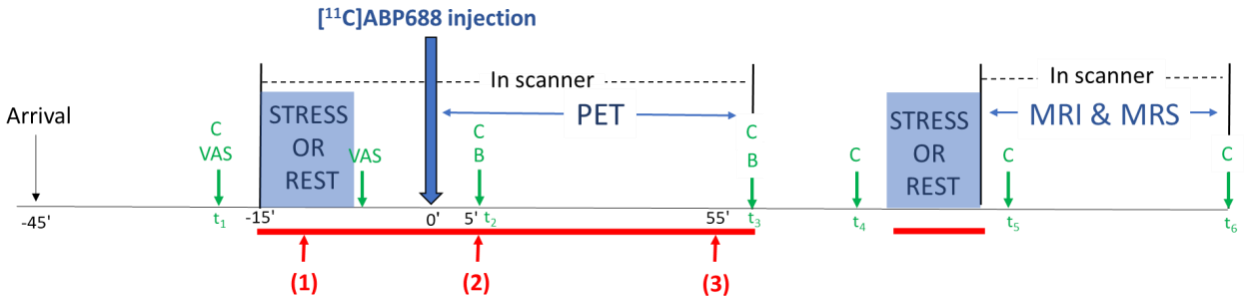

Figure 2.2: Timing of test sessions. X-axis denotes time relative to injection at time 0. Participants either went the stress or rest task within 15min before initiating the PET and MR scans. Mood ("VAS") and physiological data ("B": Il-1β measurement; "C": cortisol measurement) were collected at different time points. The red bars represent time intervals during which electrodermal activity has been tracked.

2.3 Behavioral assessment

Subjective ratings of mood, anxiety, and alertness were measured using the state-trait anxiety inventory (STAI)-State (103) and visual analog scale (VAS) of alertness. Each scale was collected two times each session, before and immediately after the first stress task (Fig. 2).

2.4 Neuroimaging

Participants were asked to refrain from consuming alcohol or medication with the exception of hormonal contraception for 1 day before scanning. On the day of the scan, they were asked to wake

up at least 4 hours prior to scanning, and to refrain from physical activity for 1 hour before scanning. Additionally, they were allowed to take no more than their usual amount of caffeine at least 4 hours before scanning and abstained from food or water for 1 hour before scanning. Prior to the scans, a urine toxicology screen for illicit drugs of abuse (Triage, Biosite Diagnostics, San Diego, CA) was performed, and a urine pregnancy test was performed in women. Participants were instructed to remain awake, rest quietly and not to move during the scan.

Synthesis of 3-(6-methyl-pyridin-2-ylethynyl)-cyclohex-2-enone-O-11C-methyl-oxime (^{11}C-ABP688) followed a procedure previously described (6), with a radiochemical of purity > 99%. All PET scans were performed conducted/obtained using a High-Resolution Research Tomograph (HRRT; Siemens/CTI, Knoxville, TN, USA), dedicated brain scanner, which combines high spatial image resolution of approximately 2-mm full width at half maximum (FWHM) (at the center of the field of view) with high sensitivity. Scans consisted of a 60-minute dynamic acquisition collected with the scanner in list-mode format, followed by a 6-minute ^{137}Cs rotating point source transmission scan for attenuation correction. The acquisition was binned into frames, which durations consisted of the following sequence: 3 × 10s, 5 × 30s, 4 × 60s, 4 × 120s, 5 × 300s, 2 × 600s. The scan initiated concurrently with the beginning of the venous injection of 370 MBq ^{11}C-ABP688 through an intravenous catheter installed at the participant's right arm vein (antecubital region).

For PET/MR anatomical co-registration, identification of regions of interests (ROIs), and spectroscopy voxel placement, all subjects also underwent high- resolution T1-weighted MRI scan after each PET session. Scans were acquired in a 3T Siemens TRIO Magneton scanner (Siemens Medical Solutions, Erlangen, Germany), using an ADNI-3D MPRAGE protocol. Images were acquired in 3D repetition time (TR) = 2300 ms, echo time (TE)= 3.42 ms, flip angle

= 9°, field of view = 256 mm, and FOV = 256 × 256; 1 mm resolution isotropic resolution. During the same session, MR spectroscopy scanning was conducted in two volumes of interests from which measures of combined glutamate (Glu) and glutamine (Gln), referred to as Glx, and Glu alone were obtained. Spectroscopic voxels were prescribed from anatomic images: a 20 x 15 x 10 mm^3 voxel was placed bilaterally over the ACC, immediately anterior to the rostrum of the corpus callosum, and perpendicular to the infra-callosal line. The striatum voxel was 25 x 12 x 12 mm^3 in size, encompassing the right dorsal caudate-putamen. The water suppressed proton spectra were acquired using a 90˚-180˚-180˚ (PRESS) sequence (TR =3000 ms, TE= 40 ms,), giving a total of 196 acquisitions. A water-unsuppressed reference scan to enable correction for eddy current- induced phase shifts was obtained immediately after the water-suppressed scan using the same TR, TE, voxel position and shim settings with 16 acquisitions. Quantification of spectra was performed using LCModel software using the raw digital MRS data. Metabolite concentrations will be expressed relative to intravoxel creatine (Cr).

2.5 PET and MRS analysis

CIVET pipeline (https://www.bic.mni.mcgill.ca/ServicesSoftware/CIVET/) (104) was used to preprocess the native MRI image. This consists of correction for intensity non-uniformity, affine transformation based on 12 parameters and non-linear normalization into standardized stereotaxic space using the high-resolution ICBM template (105) as reference. Subsequently, the resampled images were classified into white matter (WM), grey matter (GM), cerebrospinal fluid and segmented in the main brain structures and automatically labeled, using the ANIMAL probabilistic atlas-based algorithm (106). Then, the PET images emission data and the subject's own T1-weighted MRI were co-registered using a rigid-body transformation based on 6 parameters and visually inspected. Finally, the images were transformed into the Montreal Neurological Institute

template brain using transformed parameters obtained from the registration of MRI to MNI152 space. They were then normalized for the regional intensity from the cerebral gray matter to generate standard uptake value ratio images, and ^{11}C-ABP688 non-displaceable binding potential (BP_{ND}) values were estimated at each voxel using the simplified reference tissue method (SRTM), with the cerebellar grey matter as reference region. Voxel-wise BP_{ND} maps were smoothed with an 8-mm full-width at half maximum using a Gaussian filter. In a region of interest (ROI) analysis, mean BP_{ND} values were derived from time-activity curves in 9 pre-defined regions with high mGlu5 receptor expression and presumed involvement in stress response. Subcortical limbic regions amygdala and hippocampus were yielded by the segmentation generated by the ANIMAL image registration algorithm. A standard mask was used to functionally segment the striatum into ventral (VST), associative (AST), and sensorimotor (SMST) subregions, as proposed by Mawlawi et al. (107). Remaining cortical ROIs, comprising the medial (mPFC) and dorsolateral (dlPFC) prefrontal cortices, the orbitofrontal cortex (OFC), and the anterior cingulate cortex (ACC), were manually drawn on a template MRI in stereotaxic space using the software DISPLAY (http://www.bic.mni.mcgill.ca/software/Display/Display.html) and was based on the approach defined by Abi-Dargham et al. (108).

2.6 Statistics

Shapiro–Wilk tests established normal distribution of all data. The effect of stress on subjective anxiety and physiological measurements (cortisol and IL1- β) were identified using repeated measures two-way ANOVAs or mixed- model analyses when data were missing, with sessions (rest vs. stress) and timepoints as within-subject factors. Simple-main effects analyses followed when indicated. Planned pair-wise t-tests were carried out to identify differences in the magnitude of SCR and non-stimuli SCR relative to the non-specific SCRs. Summary BP_{ND} values were

computed as the unweighted mean of all examined regions in order to assess the effects of tracer and scan characteristics (mass of tracer injected per kilogram body weight and time of injection). Relationships between BP_{ND} and scans characteristics were assessed using Pearson's *r*. To test the main hypothesis of differences in BP_{ND} between conditions, separate Condition x Region x Hemisphere repeated measures ANOVAs were performed for (i) striatal regions (VST, AST, SMST), (ii) prefrontal regions (mPFC, DLPFC, OFC, and ACC), and (iii) limbic regions (amygdala and hippocampus). These were followed by planned, uncorrected two-tailed dependent measures t-tests to assess each contrast in the selected ROIs between conditions. For each ROI, percent change from scan 1 to scan 2 (($BP_{NDSTRESS} - BP_{NDREST}$)/ $BP_{NDREST} \times 100\%$) was calculated for each participant. Parametric maps of BP_{ND} were compared in voxel-wise paired *t*-tests from scan 1 to scan 2 in each participant using RMINC with a significance threshold of $p<0.05$, corrected for false discovery rate. To determine the significance of detected metabolites concentration differences due to shock administration, a Condition (rest, stress) by Region (ACC, striatum) two-way repeated measure ANOVA was applied to the MRS data. Finally, potential associations of mGlu5 receptor availability with behavioral and physiological variables were examined using Pearson's r. Given the large number of correlations performed, the unadjusted alpha level was divided by the number of studied ROIs, which resulted in a significance threshold of $p = 0.05/9 = 0.0056$. In a secondary voxel-wise analysis, further exploratory correlations using mGlu5 binding across the whole brain were assessed with parameters which revealed to be significantly correlated with ROI-wise BP_{ND}.

RESULTS

3.1 Scans and participants characteristics

Thirty-nine volunteers underwent a pre-screening telephone interview, 19 of whom were invited to a face-to-face interview. Five men and four women met the entry criteria, and all completed the study (age: 25.1±6.0 years). All were non-smokers and reported no illicit drug use during the past year. One participant was removed from the GSR analysis because of malfunction of an electrode during one scan and one was excluded from MR spectra analysis due to poor spectral fit. Three participants were removed from the saliva cortisol analysis because of one to three unusable samples.

The two PET test sessions did not differ in injected tracer dose (rest: mean 10.24 mCi, range 9.6-10.6 mCi; stress mean 10.51 mCi, range 9-11 mCi; $t(8) = -1.16$, $p = 0.28$), specific activity (rest: mean 89.32 GBq/μmol, range 23.1-128 GBq/μmol; stress mean 94.1 GBq/μmol, range 24-163.6 GBq/μmol; $t(8) = 1.204$, $p = 0.26$), or start time (rest: mean 12:30, range 11:07-15:03; stress: mean 12:37, range 11:03-14:08; $t(8) = -0.28$, $p = 0.79$). Global BP_{ND} values were not related to the mass of [^{11}C]ABP688 injected ($r = 0.22$, $p = 0.37$) or time of injection ($r = 0.27$, $p = 0.79$).

3.2 Objective indices of stress response

Skin conductance responses were significantly higher following exposure to the stressor compared to rest (two-tailed t-test, $t(7) = 4.65$, $p = 0.0023$). Phasic increases also occurred when shocks were expected, but not given, though this effect was significant at the trend level only (two-tailed dependent t-test, $t(7) = 2$, $p = 0.09$) (Fig. 3.1). Twenty minutes after initiation of the task, skin

conductance levels remained elevated (two-tailed t-test, t(7) = 3, p = 0.04) before normalizing after an hour (t(7) = 0.047, p = 0.96).

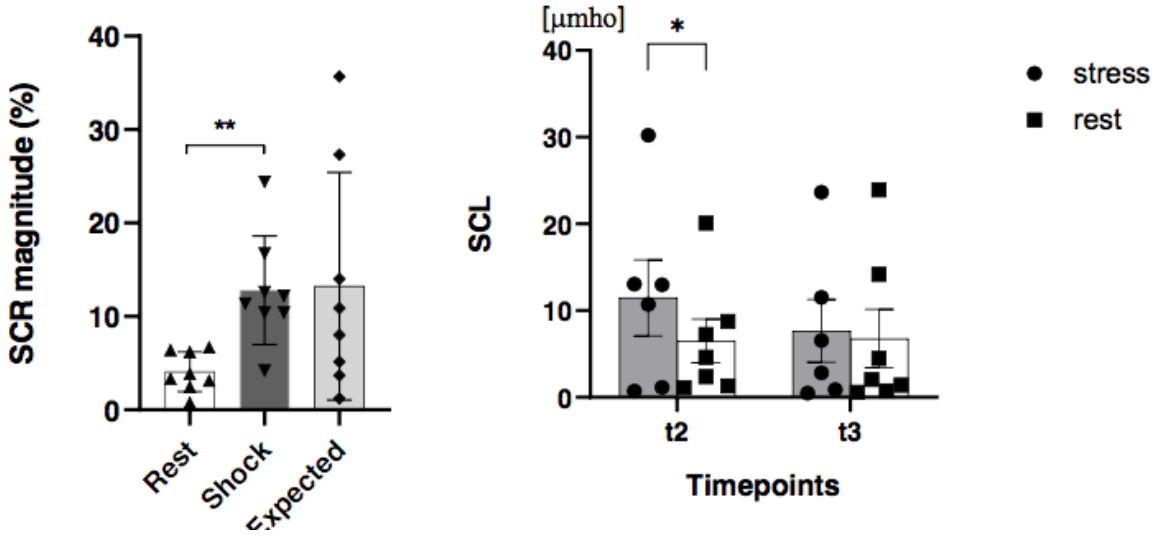

Figure 3.1: (a) The Skin Conductance Response was significantly higher during shock exposure than rest. The peak that occurs when shocks were expected but not given also showed trend-level effects reflecting higher peaks than at rest. **(b)** 20min after the initiation of shocks SCL remained higher than at rest, but this effect did not persist after an hour. Values represent mean ± S.E.M.

Saliva cortisol values did not differ significantly across conditions or time (ps>0.29; Fig. 3.2), but exploratory analyses comparing AUCi between stress and rest reached statistical significance (t(7) = 2, p = 0.041), reflecting cortisol levels that increased during the stress session ($AUCi_{STRESS}$ = 6.97) and decreased during the rest session ($AUCi_{REST}$ = -6.83). The stress-induced percent increases in cortisol and skin conductance levels were significantly correlated (r=0.838, p=0.009).

A two-way ANOVA of the Il-1β data yielded a trend level effect for session (F(7,1) = 5.3, p = 0.055). Simple main effects analyses revealed that Il-1β values tended to be higher starting from 60 min after initiation of the stress task relative to rest (p = 0.0826). The AUC_I for each condition were not significantly different (t(7) = 1.5, p = 0.176).

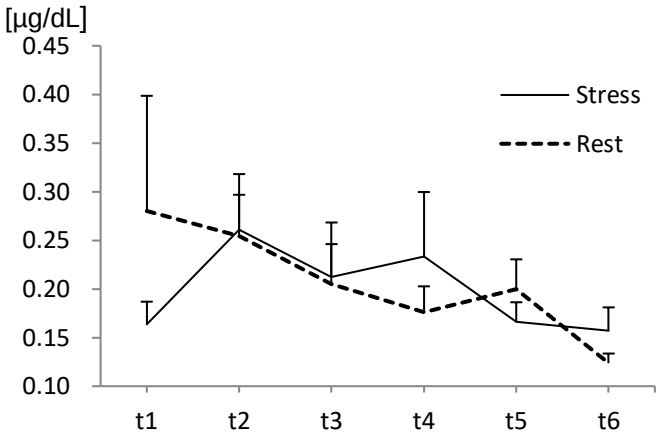

Figure 3.2: Evolution of cortisol concentrations (µg/dL) in "stress" (plain line) and "rest" (dashed line) conditions through the 6 time points of collection. t_1 and t_4 are the baseline, t_2 and t_5 were collected 20 min after initiation of the first task and repeated task respectively, and t_3 and t_6 were collected at the end of the PET and MR scans, respectively. Values represent mean + S.E.M.

3.3 Self-report measures

Two factor (Condition x Timepoints) within-subject ANOVAs yielded significant interactions for the "alert" ($F(1,7) = 9.471$, $p = 0.018$) and "anxious" VAS measures ($F(1,7) = 6.25$, $p = 0.041$), but not "afraid" ($F(1,7) = 3.3$, $p = 0.11$). Simple main effects tests revealed that in the stress condition, alertness and anxiety ratings were higher post-stress (t_2) relative to pre-stress (t_1) (alert: $t(7) = 3.784$, $p = 0.0137$; anxious: $t(7) = 3.005$, $p = 0.0396$, respectively; Fig. 3.3).

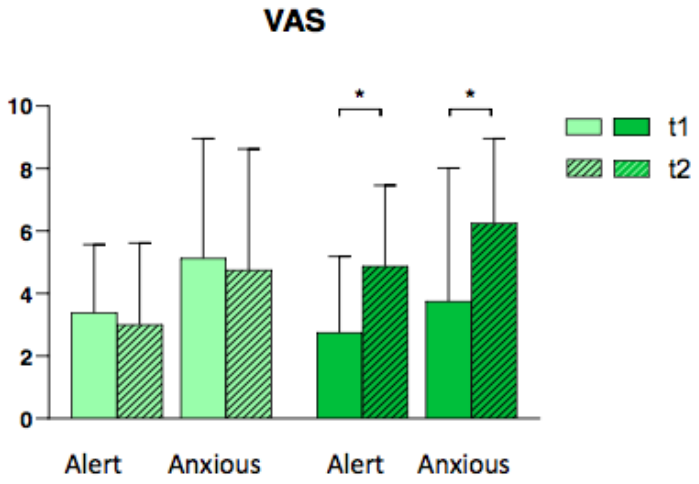

Figure 3.3: Anxiety and alertness rating was significantly higher after administration of the stress task relative to before administration and relative to baseline. Plain bars represent pre- task. Hashed bars represent post task. Light green indicates rest session, dark green indicates stress session. Values are mean ± S.E.M.

3.4 PET data

Figure 3.4 shows the time-activity curves of a representative individual in a high binding region (ACC) and in the reference region (cerebellum). Throughout the brain, regional tracer uptake reflected the known distribution of mGlu5 receptors with the highest binding in mGlu5 rich regions, such as limbic striatum and amygdala, and lower binding in the thalamus. Within each ROI, $BP_{NDSTRESS}$ and BP_{NDREST} values were positively correlated (ps < 0.04), with the exception of the OFC (p = 0.92).

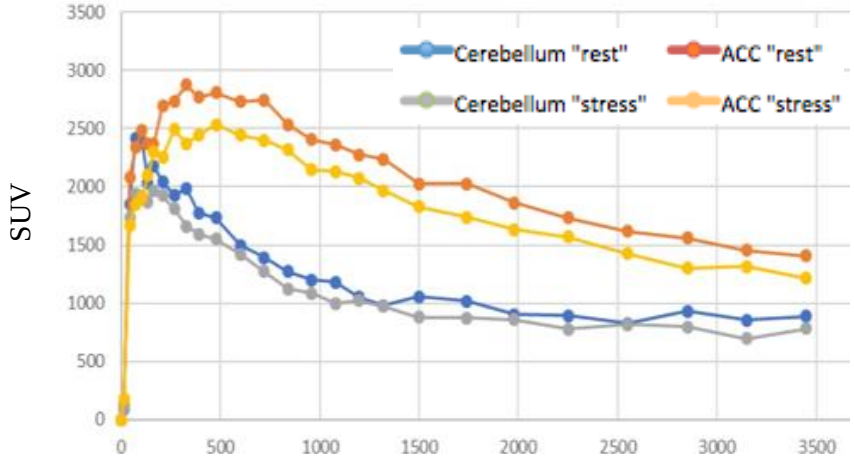

Figure 3.4: Relative time-activity curves (TACs) in "stress" and "rest" conditions of the reference region (cerebellum) and of a high binding region (anterior cingulate cortex, ACC) normalized by injected dose and body weight in one representative individual. SUV: standardized uptake value. Orange curve: TAC of ACC in the "rest" condition; yellow curve: TAC of ACC in the "stress" condition; blue curve: TAC of cerebellum in the "rest" condition; grey curve: TAC of cerebellum in the "stress" condition.

Within cortical regions, the repeated measures three-way ANOVA revealed a highly significant main effect of Subregion ($F_{3,24}$=27.9, p<0.0001), but no effects of Condition or interactions (Fs<0.97, ps>0.41). In comparison, the limbic region ANOVA yielded a highly significant Region x Hemisphere interaction ($F_{1,8}$=32.8, p<0.001). Similar results were seen when exploring the remaining striatal regions, with a significant Region x Hemisphere interaction ($F_{2,16}$=4.5 p=0.029). Simple effect tests computed on Hemisphere over Subregion within limbic and striatal regions

respectively found significantly higher binding in the left amygdala ($F_{1,15}$ =72.4, p<0.0001) and left limbic striatum ($F_{1,23}$=5,p=0.036), relative to the right side. Thus, with the exception of the amygdala and the limbic striatum, both hemispheres were averaged for further analysis. Controlling for the day of the stress session (stress session in the first scan vs. second scan) did not affect the above results. Likewise, replacing the "Condition" factor by the "Day" factor (first scan vs. second scan) did not change the results. Percent change in BP_{ND} (($BP_{ND\ STRESS}$ - $BP_{NDBASELINE}$/ $BP_{NDBASELINE}$)* 100), calculated and averaged across all ROIs within a subject, ranged from -17.5% to 18.6% (fig. 3.5). Despite individual data indicating both increases and decreases within regions, most subjects (7 of 9) had higher average binding on the stress session. A global tendency of increase was also found across regions (Positive change values, Table 3.1) but this trend did not reach conventional levels of significance in post-hoc pairwise comparisons (ps>0.3, uncorrected). Voxel-wise parametric analyses were consistent with these findings, with no clusters of significant voxels emerging.

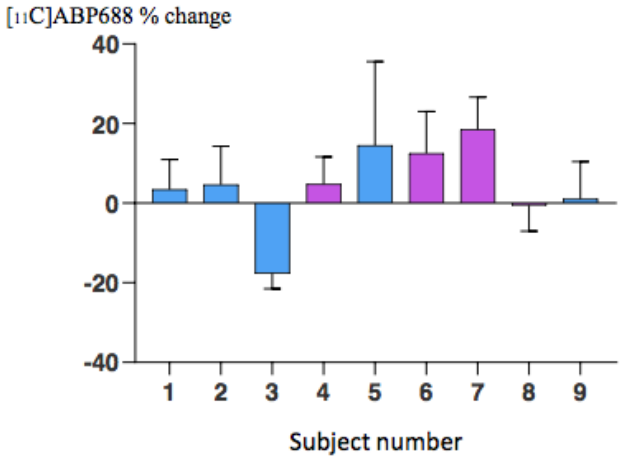

Figure 3.5: Mean percent change [11C]ABP688 BP_{ND} were averaged over nine regions: anterior cingulate, medial prefrontal cortex, orbitofrontal cortex, ventral striatum, associative striatum, sensorimotor striatum, amygdala and hippocampus. Blue bars represent male subjects. Violet bars represent female subjects. Values are mean ± S.E.M.

Although subsamples were small, we looked for possible sex differences. A two-way sex by test condition ANOVA performed for BP_{ND} values in subcortical limbic, striatal and prefrontal regions yielded a significant main effect of sex in limbic and striatal regions (limbic: $F(1,6)=44.57$, $p=0.0005$; striatal: $F(1,6)=7.59$, $p=0.03$), reflecting higher binding in males than in females at rest (limbic: $p=0.001$; striatal: $p=0.028$) and also at stress in limbic regions ($p=0.0005$). Mean magnitude of increase was 34% across regions.

Table 3.1: [^{11}C]ABP688 BP_{ND} values in each ROI during the stress and control sessions, and mean extent of change from stress to rest.

Region	**Rest BP_{ND} (mean ± SD)**	**Stress BP_{ND} (mean ± SD)**	**Mean % difference**	**p**
Cortex	1.09 ± 0.24	1.13 ± 0.16	+5%	0.48
mPFC	1.23 ± 0.28	1.27 ± 0.18	+6%	0.61
dlPFC	1.01 ± 0.21	1.05 ± 0.16	+6%	0.32
ACC	1.19 ± 0.28	1.2 ± 0.2	+3%	0.98
OFC	0.92 ± 0.24	0.98 ± 0.14	+11%	0.30
Striatum	0.87 ± 0.17	0.89 ± 0.1	+5%	0.32
Associative	1.02 ± 02	1.08 ± 0.13	+1%	0.96
Ventral	1.15 ± 0.24	1.2 ± 0.17	+4%	0.82
Sensorimotor	0.87 ± 0.15	0.87 ± 0.1	+4%	0.21
Limbic subcortical	0.93 ± 0.2	0.92 ± 0.14	+1%	0.8
Amygdala	1.04 ± 0.26	1.02 ± 0.16	+0%	0.64
Hippocampus	0.81 ± 0.19	0.81 ± 0.13	+3%	0.67
Summary BP_{ND}	1.03 ± 0.17	1.05 ± 0.15	+5%	

BP_{ND}, binding potential, non-displaceable; dlPFC, dorsolateral prefrontal cortex; OFC, orbitofrontal cortex; ACC, anterior cingulate cortex; mPFC, medial prefrontal cortex.

3.5 MRS data

Figure 3.6 shows a representative spectrum of the MRS outcome measures. The glutamate level index did not significantly change from baseline to stress in either region (main effect of Session: $F(1,7) = .25$, $p = 0.63$; Session x Region interaction: $F(1,7) = 0.87$, $p = 0.38$). The combined Glutamate + Glutamine (Glx) levels exhibited more variability (Fig. 3.7, Table 2), including relative increases of 2% in the ACC and 13% in the striatum. These changes did not yield a significant effect of Session ($F(1,7) = 1.09$, $p = 0.33$) but a trend level Region x Session interaction was seen ($F(1,7) = 0.16$, $p = 0.08$). Post-hoc tests yielded a significant stress-induced increase in Glx concentrations in the striatum ($p=0.048$) but not in the ACC ($p=0.5$) (Fig. 3.6, Table 3.2).

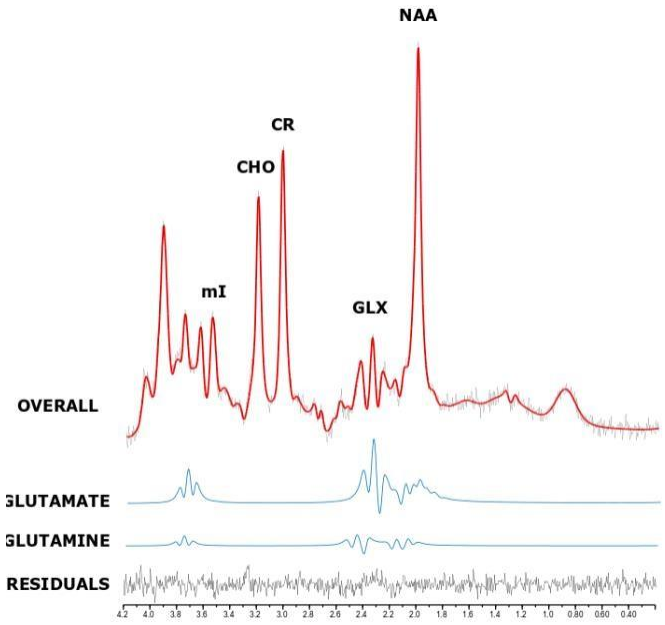

Figure 3.6: Example spectra of MRS measurement in the stress condition from one participant. The grey curve is the original spectrum and residuals. The red curve is the fitted spectrum from LCModel. Blue curves mark Glu and Gln contributions to the overall spectrum. Higher spectral contribution of glutamate, in line with higher intra-cellular concentration of glutamate relative to glutamine.

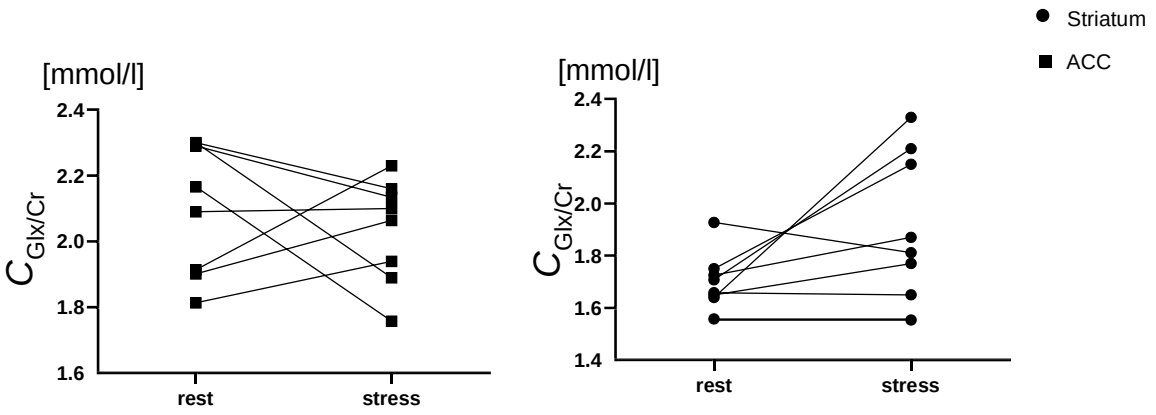

Figure 3.7: Changes from rest scan to stress scan in combined glutamate and glutamine concentrations (mmol/L) for each participant in the Striatum (circles) and the Anterior Cingulate Cortex (squares).

	Rest	**Stress**	**Rest**	**Stress**
	Striatum		***ACC***	
Glutamate				
C_{Glu} [mmol/l]	10.9 ± 1.65	10.8 ± 1.36	10.5 ± 0.8	9.8 ± 0.77
$C_{Glu/Cr}$ [mmol/l]	1.3 ± 0.2	1.4 ± 0.19	1.7 ± 0.16	1.6 ± 0.1
$\Delta C_{Glu/Cr}$ [%]		+4%		-4%
Glx				
C_{Glx} [mmol/l]	13.6 ± 1.17	14.7 ± 1.73	12.8 ± 1.12	12.2 ± 1.25
$C_{Glx/Cr}$ [mmol/l]	1.7 ± 1.9	1.9 ± 1.3	2.1 ± 0.2	2 ± 0.16
$\Delta C_{Glx/Cr}$ [%]		+13%		-2%
Glx/Glu				
$C_{Glx/Glu}$ [mmol/l]	1.26 ± 0.16	1.38 ± 0.2	1.22± 0.06	1.25 ± 0.05
$\Delta C_{Glx/Glu}$ [%]		10%		2%

Table 3.2: Absolute concentrations and concentrations relative to creatine of glutamate and total glutamate and glutamine (*Cx*: mean ± std in mmol/l) for the two conditions, "stress" and "rest". Δ*Cx* denotes changes of concentrations (in %) for the stress condition relative to the rest condition.

3.6 Correlations

Correlational analysis did not identify significant associations between stress-induced changes in BP_{ND} values and stress-induced changes in Glx/Glu ratios (Table 3.3) or between BP_{ND} values and Glx/Glu ratios at rest (Table 3.3). However, BP_{ND} values on the stress session ($BP_{NDSTRESS}$) in limbic, sensorimotor and associative striatum, OFC and left amygdala were negatively correlated with stress-induced changes in Glx/Glu levels in the ACC ($rs > -0.71$, $ps < 0.044$, uncorrected. See Table 3.3). $BP_{NDSTRESS}$ values were also associated with Glx/Glu levels in the ACC at stress in the ACC and both associative and sensorimotor striatum ($rs > -0.43$, $ps < 0.036$, uncorrected. Table 3.3). These associations should be interpreted cautiously as they were not significant once adjusted for the nine ROI ($0.05/9 = 0.0056$). Finally, individual differences in the cortisol $AUCg_{STRESS}$ response were negatively correlated with $BP_{NDSTRESS}$ values in the amygdala, ACC, OFC, and limbic striatum ($rs < -0.71$, $ps < 0.048$, uncorrected), and to a lesser extent in the hippocampus ($r=-0.7$, $p=0.054$, uncorrected). Stress-induced changes in the cortisol AUCg were also correlated with $BP_{NDSTRESS}$ values in the striatum, OFC, amygdala and hippocampus ($rs < -0.72$, $ps < 0.045$, uncorrected). Correlations that survived at $p=0.0056$ are shown in Figure 3.8. Consistent with the ROI analyses, the whole-brain correlational analysis identified negative associations between $BP_{NDSTRESS}$ values in subcortical limbic regions and both ACC Glx/Glu levels on the stress session and ACC Δ Glx/Glu. This brain-wide analysis also identified a significant association between and the left sensorimotor area, corresponding to the contralateral side of the participants' wrist where the shocks were given. No correlations were found with other physiological parameters and psychological parameters.

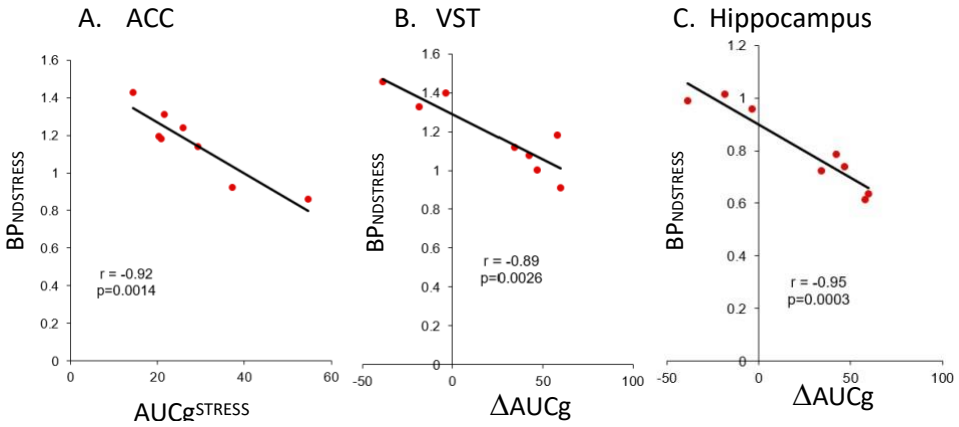

Figure 3.8 (A-C): **Association between mGlu5 availability on the stress session and cortisol AUCg^{STRESS} response (panel A) and changes in cortisol AUCg (panels B-C).** A: Anterior Cingulate Cortex. B: Right ventral (limbic) striatum. Regions which demonstrated significance at $p \leq 0.0056$ are showed.

Table 3.3: Pearson correlation among [$_{11}$C]ABP688BP$_{ND}$, Glx/Glu ratios and cortisol AUCg values.

Variables		Stress		Stress-induced change		Rest	
		AUCg	Glx/Glu	AUCg	Glx/Glu	AUCg	Glx/Glu
Stress	*ACC*	.0014[b]	.068	.2	.38		
	OFC	.048[a]	.34	.029[a]	.039[a]		
BP$_{ND}$	*Amygdala*	.0014[a] (right)	.034[a]	.011[a]	.027[a] (left)		
	Hippocampus	.054	.13	.0003[b]	.12		
	VST	.029[a] (left)	.03[a] (right)	.0026[b] (right)	.0094[a]		
	AST	.067	.035[a]	.03[a]	.044[a]		
	SMST	.075	.24	.01[a]	.009[a]		
Stress-induced change	*ACC*			.074	.078		
	OFC			.26	.36		
	Amygdala			.1	.29		
BP$_{ND}$	*Hippocampus*			.38	.32		
	VST			.27	.25		
	AST			.11	.15		
	SMST			.26	.31		
Rest	*ACC*					.8	.067
BP$_{ND}$	*OFC*					.28	.11
	Amygdala					.63	.75
	Hippocampus					.68	.75
	VST					.11	.24
	AST					.35	.48
	SMST					.32	.52

[a]: correlation is significant at p = 0.05.

[b]: correlation is significant at p = 0.0056, corrected for multiple testing.

DISCUSSION

The study's primary goal was to test whether acute stress-induced glutamate release could be measured in humans using PET with [^{11}C]ABP688 and magnetic resonance spectroscopy (MRS). The self-report and physiological measures indicated that the stress paradigm was effective. Exposure to the wrist shock led to increased self-reported anxiety and skin conductance responses (SCRs) over and above the first resting measure (AUCi). However, these effects were not large. Potentially related to this, exposure to the laboratory stressor did not lead to significant decreases in [^{11}C]ABP688 BP_{ND} values and induced only a weak effect on a secondary measure with MRS.

To the extent that changes in [^{11}C]ABP688 binding values occurred, they were small (less than 6%), within our previously reported range of the test–retest variability (11 to 21%), and, on average, in the opposite direction to that predicted. In part, this reflected marked individual differences in the responses. This variability might reflect more than statistical noise. Indeed, exploratory analyses identified negative correlations between stress-induced increases in salivary cortisol and BP_{ND} values in the amygdala, ACC, OFC, and limbic striatum on the stress session. Since, however, correlations were not seen with stress-induced changes in BP_{ND} values, the above associations should be interpreted cautiously.

The MR spectroscopy analyses tentatively identified a weak stress-induced increase in the striatal tissue Glx signal without an accompanying change in glutamate (Glu). An increase in Glx in the absence of increased Glu is thought to index elevated glutamine metabolism (Gln) (41), possibly reflecting stress-induced glutamate release, enhanced glial glutamate uptake, and increased conversion to Gln. These responses were not seen in the ACC, but the stress-induced changes in the ACC Glx to Glu ratio were correlated with stress session BP_{ND} values in the ACC and striatum;

the greater the Glx/Glu change, the lower the BP_{ND} values. Again, these associations need to be interpreted cautiously.

The current study was conducted based on the possibility that the PET [^{11}C]ABP688 method can detect changes in extracellular glutamate levels. Using the tool in this way has some support but is controversial. The standard for validating a PET tracer as a tool to measure neurotransmitter release is to demonstrate that changes in binding are proportional to microdialysis measured changes in neurotransmitter release. This proportional association has yet to be reported, but several studies in laboratory animals have investigated the influence of extra-cellular glutamate on the binding of tracers that bind to the mGlu5 receptor allosteric site, most of them using drugs that either provoke a glutamate surge (44,45,79,109,110) or reduce synaptic glutamate concentrations (80). Most of them found lower and higher mGlu5 availability respectively, with the exception of one study using ketamine (109) and another one with N-acetyl Cysteine and MK-801 (110).

The relation between changes in mGlu5 receptor availability and MRS measures of glutamate has been tested in clinical populations including a study measuring binding differences between cocaine-dependent and healthy subjects (74) and another one comparing MDD to healthy subjects (38). While the first study did not find a correlation between the two measures, in the latter, MRS measured glutamate turnover in the ACC in the patient cohort was significantly correlated with [^{18}F]FPEB binding, another PET tracer that binds to the same site as [^{11}C]ABP688. Thus, this constitutes the first *in vivo* evidence of glutamatergic influence on mGlu5 availability (38). However, in this study (38), in contrast to our study or pharmacological challenges assessing the immediate effects of a rapid glutamate surge, the results likely reflected long term effects of elevated glutamate level on receptor availability, because post-mortem evidence from the tissues of patients with a history of depression suggests that reduced mGlu5 protein expression (37) might

account for the observed lower mGlu5 availability. Hence, the nature of the alteration that eventually leads to changes in mGlu5 availability probably differs. Nevertheless, we also found associations between [$_{11}$C]ABP688 BP_{ND} values on the stress session with ACC Glx:Glu values at stress, as well as with stress-induced changes in ACC Glx:Glu values. However, these correlations did not survive multiple comparisons, somewhat limiting the generalizability of the findings.

The lack of a significant correlation between [$_{11}$C]ABP688 BP_{ND} values and MRS measures at rest might be surprising given the similar mGlu5 receptor availability on the two test sessions. This might reflect, in part, the narrower range of MRS values seen at rest relative to the stress session. It is also possible that BP_{ND} values on the rest scan were affected by the novelty of the scanning environment, for those participants who had their rest scan on day 1. Alternatively, the participants in whom shocks were administered on day 1 may have developed stressful associations with the testing environment and might have expected to receive shocks on their rest scan too. Nevertheless, our measures of stress response and MRS findings do not suggest that stress levels were elevated on the control test session. Instead, it is plausible that the novelty stress effect globally affected subjects' first scanning experiences, overlapping with the task-related stress in the stress session and altering baseline stress levels in the rest session. This might have added additional noise to the data. To test for this possibility, we compared data between the first versus second scan. However, we did not find evidence for elevated BP_{ND} in the second scan (data not shown). This noted, to more effectively rule out this potential confound in future studies, investigators should familiarise participants to the scanning environment during a first visit.

Limitations

When interpreting our mostly negative findings, the following features should be considered. In most participants, pain ratings exhibited more variation than expected across the three sessions (screening assessment, PET stress session, MRS stress session). As a consequence, voltage thresholds had to be recalibrated at the beginning of each task. Pain ratings also differed between each stimulus of equal intensity from the same block, making it difficult to maintain an accurate threshold level. It is therefore possible that the present study's shocks were not sufficiently stress-inducing to evoke a detectable change in glutamate. A previous MRS study using chemically induced stress that identified more compelling glutamate responses saw effects that peaked in the tens of minutes following an acute stressful stimulus (35) and may have persisted for several hours (8,111,112).

On the stress test day, the wrist shock was administered twice, immediately before the PET and before the MRS scans. This was intended to elicit similar psychophysiological states in the PET and MRS. However, it is possible that the different environments or expectations produced different responses. Moreover, the repeated stress exposure study design may have led to either sensitized or habituation responses. Consistent with a within-session habituation effect, subjects reported decreasing VAS measured stress scores during the stimulation session. If the stressor induced variable effects ranging from almost no aversion to relatively fear-inducing, this might explain the heterogenous stress-induced changes in Glu and Glx levels, ranging from to -29% to 42%. A simultaneous PET/MRI would have diminished some of these issues by avoiding the need to repeat the stress task. This type of scanner was not available.

The administered electrical stimulation has little resemblance to ordinary life stressors, limiting the generalizability of the findings. It is possible that glutamate levels are less susceptible to this

type of stressor as to daily life stressor or pharmacologically-induced stress (35). Future research can build on the present work by expanding it to psychosocial stress paradigms. That said, a recent high magnetic field strength MR study using the Trier Social Stress Test did not detect any alterations in medial prefrontal glutamate nor GABA level (36). This might highlight the challenges of testing and reproducing psychosocial paradigm in human experiments. The responses to stressors are potently influenced by cognitive appraisals of the experience, leading to marked individual differences (113). As such, large inter-individual variations in stress responses have been frequently reported (114,115).

The [^{11}C]ABP688 PET measure might also have been sub-optimal. Much unexpected variability in the signal has been reported. The present study was initiated based on the possibility that this variability indexed changes in glutamate release. The mechanisms accounting for this hypothesized effect remain to be elucidated, but could include alterations in membrane protein expression, receptor trafficking, dimerization or conformation changes.

Irrespective of the mediating mechanisms, PET [^{11}C]ABP688 studies have yielded stable test-retest binding measures in anesthetized rats (116) but not in nonhuman primates (71,79,81) or humans (82,86,117). Human studies have found within-subject variation as high as 73%, with an average variation of 23-39% in regional BP_{ND} (117) and changes across regions of approximately -50 to 140% (82). Low reliability persisted when the experiment was repeated using [^{18}F]FPEB, another negative allosteric modulator (NAM) PET tracer that binds to the allosteric site of mGlu5 receptor, suggesting that variation in binding may be due to intrinsic characteristics of the receptor and its binding sites (82).

One source of the above variability is the time of the scan. For example, circadian variations have been reported for mGlu5 availability and glutamate levels (82,84,118). Higher binding values were

seen in a study in rodents during the sleep phase compared to the awake phase (84) and after one night of sleep deprivation in humans (118), as well as later in the day relative to morning scans in humans (82). This present study reduced time of the scan variability as much as possible, both across sessions and between individual participants (86), and time of PET tracer injection did not differ between the sessions, nor did BP_{ND} values correlate with the time of scan. Nevertheless, one participant underwent a rest scan much later in the afternoon compared to the stress scan and to the average rest scan start time due to a tracer production failure. This same subject exhibited higher binding at rest (as hypothesized), compared to other participants. Moreover, the region-averaged variations of 17% between stress and rest scans observed in this subject constitute the highest variation seen for this current study. In comparison, we recently reported that test-retest [^{11}C]ABP688 BP_{ND} values are more stable when participants are tested at the same time of day on different days (82). Thus, it is possible that many previous reports of alterations in BP_{ND} reflect circadian rhythm effects instead of stress.

A second contributing factor is variability in the (E) to (Z) [^{11}C]ABP688 isomer ratio. Even a modest level of (Z)-isomer content can decrease [^{11}C]ABP688 measures (65,67). The present study benefited from a production protocol recently developed by our lab that yields diastereomerically pure (>99%) (E)-[^{11}C]ABP688 content (68). Differences in specific activity were also taken into account (119) and had no correlations with binding values. Thus, the variations in tracer binding observed in the present work were not explained by any of these technical factors.

A third contributing factor is sex. This is now a consistent finding in our laboratory, both in large (120) and small samples (22) (current study). This sex difference has also been observed elsewhere by some (75) but not all groups (37,77). The most parsimonious explanation for the discrepant results is that we control for variability in the data introduced by (Z)-isomer content, either by

using the isomer ratio as a covariate (22,67,120) or by using diastereomerically pure (>99%) (E)-[^{11}C]ABP688 (current study).

Fourth, the use of cerebellum as a reference region to compute BP_{ND} values is not without controversy. Two in vivo competition studies measuring tracer retention using a blocking agent identified an effect in the cerebellum (121,122), and it has been shown that the non-specific distribution volume (DV) for [^{11}C]ABP688 is only one-third of the total DV (66). Thus, although outcome measures yielded by SRTM and arterial input function have been shown to be highly correlated (74), [^{11}C]ABP688 exhibits some specific binding in the cerebellar grey matter which makes this region still the most suited, but not the ideal reference region. The existence of even subtle specific binding can lead to underestimations in measured BP_{ND} variations (82), as compared to outcome measures yielded by using an arterial input function. While we were expecting to see substantial differences in TAC obtained for the ROIs and subtle to no differences in the reference region TAC, we roughly saw the same scale of variation between the two conditions for a high uptake region (ACC) and the cerebral grey matter. Thus, it is possible that differences in cerebellum tracer uptake could have masked real variations between stress and rest in the ROIs, and especially given that the variations in our study were not expected to be pronounced, this could have even affected the direction of the variations, thereby yielding a trend of increase instead of the opposite.

Conclusion

To conclude, acute exposure to a laboratory stressor did not induce detectable changes in mGlu5 receptor availability as measured with high-resolution HRRT PET and [^{11}C]ABP688. While [^{11}C]ABP688 has been used to measure differences in mGlu5 availability in group comparisons

studies, our study suggest that it is not a suitable tool for investigating effects of moderate extra-cellular glutamate fluctuations. However, by combining MRS and PET data, we saw preliminary evidence that the two measures might be related, even though a shift in glutamate turnover may not be the primary driver of differences in the tracer binding. Together, the results suggest that the sensitivity of [$_{11}$C]ABP688 to extracellular glutamate manipulation cannot be discounted and requires further investigation.

REFERENCES

1. McEwen BS. Physiology and neurobiology of stress and adaptation: Central role of the brain. Physiol Rev. 2007 Jul 1;87(3):873–904.

2. McEwen BS, Gianaros PJ. Stress and allostasis-induced brain plasticity. Annu Rev Med. 2011;62:431–45.

3. Moghaddam B. Stress activation of glutamate neurotransmission in the prefrontal cortex: implications for dopamine-associated psychiatric disorders. Biol Psychiatry. 2002 May 15;51(10):775–87.

4. Davis MT, Holmes SE, Pietrzak RH, Esterlis I. Neurobiology of chronic stress-related psychiatric disorders: Evidence from molecular imaging studies. Chronic Stress. 2017 Dec;1:10.

5. Averill LA, Purohit P, Averill CL, Boesl MA, Krystal JH, Abdallah CG. Glutamate dysregulation and glutamatergic therapeutics for PTSD: Evidence from human studies. Neurosci Lett. 2017 May 10;649:147–55.

6. McGonagle KA, Kessler RC. Chronic stress, acute stress, and depressive symptoms. Am J Community Psychol. 1990 Oct;18(5):681–706.

7. Luczynski P, Moquin L, Gratton A. Chronic stress alters the dendritic morphology of callosal neurons and the acute glutamate stress response in the rat medial prefrontal cortex. Stress Amst Neth. 2015;18(6):654–67.

8. Musazzi L, Tornese P, Sala N, Popoli M. Acute or Chronic? A Stressful Question. Trends Neurosci. 2017 Sep;40(9):525–35.

9. Lee AL, Ogle WO, Sapolsky RM. Stress and depression: Possible links to neuron death in the hippocampus. Bipolar Disord. 2002;4(2):117–28.

10. Vyas A, Mitra R, Shankaranarayana Rao BS, Chattarji S. Chronic stress induces contrasting patterns of dendritic remodeling in hippocampal and amygdaloid neurons. J Neurosci. 2002 Aug 1;22(15):6810–8.

11. McEwen BS. The neurobiology of stress: from serendipity to clinical relevance. Brain Res. 2000 Dec 15;886(1):172–89.

12. Liguz-Lecznar M, Skangiel-Kramska J. Vesicular glutamate transporters VGLUT1 and VGLUT2 in the developing mouse barrel cortex. Int J Dev Neurosci Off J Int Soc Dev Neurosci. 2007 Apr;25(2):107–14.

13. Hascup ER, Hascup KN, Stephens M, Pomerleau F, Huettl P, Gratton A. Rapid microelectrode measurements and the origin and regulation of extracellular glutamate in rat prefrontal cortex. J Neurochem. 2010 Dec;115(6):1608–20.

14. Dingledine R, Borges K, Bowie D, Traynelis SF. The glutamate receptor ion channels. Pharmacol Rev. 1999 Mar;51(1):7–61.

15. Anwyl R. Metabotropic glutamate receptors: electrophysiological properties and role in plasticity. Brain Res Brain Res Rev. 1999 Jan;29(1):83–120.

16. Conn PJ, Lindsley CW, Jones CK. Activation of metabotropic glutamate receptors as a novel approach for the treatment of schizophrenia. Trends Pharmacol Sci. 2009 Jan 1;30(1):25–31.

17. Pin J-P, Duvoisin R. The metabotropic glutamate receptors: Structure and functions. Neuropharmacology. 1995 Jan;34(1):1–26.

18. Niswender CM, Conn PJ. Metabotropic glutamate receptors: physiology, pharmacology, and disease. Annu Rev Pharmacol Toxicol. 2010;50:295–322.

19. Aramori I, Nakanishi S. Signal transduction and pharmacological characteristics of a metabotropic glutamate receptor, mGluRl, in transfected CHO cells. Neuron. 1992 Apr 1;8(4):757–65.

20. Nicoletti F, Bruno V, Catania MV, Battaglia G, Copani A, Barbagallo G. Group-I metabotropic glutamate receptors: hypotheses to explain their dual role in neurotoxicity and neuroprotection. Neuropharmacology. 1999 Oct;38(10):1477–84.

21. Kniazeff J, Bessis A-S, Maurel D, Ansanay H, Prézeau L, Pin J-P. Closed state of both binding domains of homodimeric mGlu receptors is required for full activity. Nat Struct Mol Biol. 2004 Aug;11(8):706–13.

22. Smart K, Nagano-Saito A, Milella M, Sakae DY, Favier M, Vigneault E, Louie L, Hamilton A, Ferguson SSG, Rosa-Neto P, Narayanan S, El Mestikawy S, Leyton M, Benkelfat C. Low metabotropic glutamate type 5 receptor binding is associated with d-amphetamine sensitization in mice and humans. Journal of Psychiatry & Neuroscience 2020 In Press.

23. Luján R, Roberts JD, Shigemoto R, Ohishi H, Somogyi P. Differential plasma membrane distribution of metabotropic glutamate receptors mGluR1 alpha, mGluR2 and mGluR5, relative to neurotransmitter release sites. J Chem Neuroanat. 1997 Oct;13(4):219–41.

24. Lujan R, Nusser Z, Roberts JD, Shigemoto R, Somogyi P. Perisynaptic location of metabotropic glutamate receptors mGluR1 and mGluR5 on dendrites and dendritic spines in the rat hippocampus. Eur J Neurosci. 1996 Jul;8(7):1488–500.

25. Shigemoto R, Nomura S, Ohishi H, Sugihara H, Nakanishi S, Mizuno N. Immunohistochemical localization of a metabotropic glutamate receptor, mGluR5, in the rat brain. Neurosci Lett. 1993 Nov 26;163(1):53–7.

26. Romano C, Yang W-L, O'Malley KL. Metabotropic glutamate receptor 5 is a disulfide-linked dimer. J Biol Chem. 1996 Nov 8;271(45):28612–6.

27. Arnsten AFT. Stress weakens prefrontal networks: molecular insults to higher cognition. Nat Neurosci. 2015 Oct;18(10):1376–85.

28. Musazzi L, Milanese M, Farisello P, Zappettini S, Tardito D, Barbiero VS, Bonifacino T, Mallei A, Baldelli P, Racagni G, Raiteri M, Benfenati F, Bonanno G, Popoli M. Acute stress increases depolarization-evoked glutamate release in the rat prefrontal/frontal cortex: The dampening action of antidepressants. PLoS ONE 2010. vol. 5, no. 1, 2010, p. e8566.

29. Rezkinov L, Grillo C, Piroli G, Pasumarthi R, Reagan L, Fadel J . Acute stress-mediated increases in extracellular glutamate levels in the rat amygdala: differential effects of antidepressant treatment. European Journal of Neuroscience. 2007 June 06 Vol.25(10), pp.3109-3114.

30. Lupinsky D, Moquin L, Gratton A. Interhemispheric regulation of the rat medial prefrontal cortical glutamate stress response: role of local GABA- and dopamine-sensitive mechanisms. Psychopharmacology (Berl). 2017 Feb;234(3):353–63.

31. Popoli M, Yan Z, McEwen B, Sanacora G. The stressed synapse: the impact of stress and glucocorticoids on glutamate transmission. Nat Rev Neurosci. 2011 Nov 30;13(1):22–37.

32. Gutzeit A, Meier D, Froehlich JM, Hergan K, Kos S, v. Weymarn C. Differential NMR spectroscopy reactions of anterior/posterior and right/left insular subdivisions due to acute dental pain. Eur Radiol. 2013 Feb 1;23(2):450–60.

33. Mullins PG, Rowland LM, Jung RE, Sibbitt WL. A novel technique to study the brain's response to pain: Proton magnetic resonance spectroscopy. NeuroImage. 2005 Jun 1;26(2):642–6.

34. Bryant RA, Felmingham KL, Das P, Malhi GS. The effect of perceiving control on glutamatergic function and tolerating stress. Mol Psychiatry. 2014 May;19(5):533–4.

35. Zwanzger P, Zavorotnyy M, Gencheva E, Diemer J, Kugel H, Heindel W, Ruland T, Ohrmann P, Arolt V, Domschke K, Pfleiderer B. Acute shift in glutamate concentrations following experimentally induced panic with cholecystokinin tetrapeptide - A 3T-MRS study in healthy subjects. Neuropsychopharmacology. 2013 Aug;38(9):1648–54.

36. Houtepen LC, Schür RR, Wijnen JP, Boer VO, Boks MPM, Kahn RS. Acute stress effects on GABA and glutamate levels in the prefrontal cortex: A 7T 1H magnetic resonance spectroscopy study. NeuroImage Clin. 2017 Jan 1;14:195–200.

37. Deschwanden A, Karolewicz B, Feyissa AM, Treyer V, Ametamey SM, Johayem A, Burger C, Auberson Y, Sovago J, Stockmeier C, Buck A, Hasler G. Reduced metabotropic glutamate receptor 5 density in major depression determined by [11C]ABP688 positron emission tomography and postmortem study. Am J Psychiatry. 2011 Jul;168(7):727–34.

38. Abdallah CG, Hannestad J, Mason GF, Holmes SE, DellaGioia N, Sanacora G, Lin X , Javitch J, Planeta B, Nabulsi N, Carson R, Esterlis I. Metabotropic glutamate receptor 5 and glutamate involvement in major depressive disorder: a multimodal imaging study. Biol Psychiatry Cogn Neurosci Neuroimaging. 2017 Jul;2(5):449–56.

39. Auer D, Puetz B, Kraft E, Lipinski B, Holsboer F. Reduced glutamate in the anterior cingulate cortex in depression: an in vivo proton magnetic resonance spectroscopy study. Biol Psychiatry. 2000; Vol.47(4), pp.305-313.

40. Sanacora G, Gueorguieva R, Epperson CN, Wu Y-T, Appel M, Rothman DL. Subtype-specific alterations of gamma-aminobutyric acid and glutamate in patients with major depression. Arch Gen Psychiatry. 2004 Jul;61(7):705–13.

41. Yüksel C, Öngür D. Magnetic resonance spectroscopy studies of glutamate-related abnormalities in mood disorders. Biol Psychiatry. 2010 Nov 1;68(9):785–94.

42. Berman RM, Cappiello A, Anand A, Oren DA, Heninger GR, Charney DS, Krystal JH. Antidepressant effects of ketamine in depressed patients. Biol Psychiatry. 2000 Feb 15;47(4):351–4.

43. Abdallah CG, Adams TG, Kelmendi B, Esterlis I, Sanacora G, Krystal JH. Ketamine's mechanism of action: a path to rapid-acting antidepressants. Depress Anxiety. 2016;33(8):689–97.

44. DeLorenzo C, DellaGioia N, Bloch M, Sanacora G, Nabulsi N, Abdallah C, J Yang, Pittenger, Sanacora G, Krystal J H, Parsey R V, Carson R E, Esterilis I. In vivo ketamine-induced changes in [11C]ABP688 binding to metabotropic glutamate receptor subtype 5. Biol Psychiatry. 2015 Feb 1;77(3):266–75.

45. Esterlis I, DellaGioia N, Pietrzak RH, Matuskey D, Nabulsi N, Abdallah CG, J Yang, Pittenger C, Sanacora G, Krystal J H, Parsey R V, Carson R E, DeLorenzo C. Ketamine-induced reduction in mGluR5 availability is associated with an antidepressant response: an [11C]ABP688 and PET imaging study in depression. Mol Psychiatry. 2018 Apr;23(4):824–32.

46. Holmes SE, Girgenti MJ, Davis MT, Pietrzak RH, DellaGioia N, Nabulsi N, Krystal JH, Esterlis I. Altered metabotropic glutamate receptor 5 markers in PTSD: In vivo and postmortem evidence. Proc Natl Acad Sci U S A. 2017 Aug 1;114(31):8390–5.

47. Schulz B, Fendt M, Gasparini F, Lingenhöhl K, Kuhn R, Koch M. The metabotropic glutamate receptor antagonist 2-methyl-6-(phenylethynyl)-pyridine (MPEP) blocks fear conditioning in rats. Neuropharmacology. 2001 Jul 1;41(1):1–7.

48. Schmidt KC, Turkheimer FE. Kinetic modeling in positron emission tomography. Q J Nucl Med Off Publ Ital Assoc Nucl Med AIMN Int Assoc Radiopharmacol IAR. 2002 Mar;46(1):70–85.

49. Heiss W-D, Habedank B, Klein JC, Herholz K, Wienhard K, Lenox M. Metabolic Rates in small brain nuclei determined by High-Resolution PET. J Nucl Med. 2004 Nov 1;45(11):1811–5.

50. Pagani M, Stone-Elander S, Larsson SA. Alternative positron emission tomography with non-conventional positron emitters: effects of their physical properties on image quality and potential clinical applications. Eur J Nucl Med Mol Imaging. 1997 Oct 14;24(10):1301–27.

51. Myers, R., Bailey D., Cunningham V., Jones T. (1996). Quantification of brain function. Academia Press, San Diego, 443 PP.

52. Li D, Shan H, Conti P, Li Z. PET imaging of metabotropic glutamate receptor subtype 5 (mGluR5). Am J Nucl Med Mol Imaging. 2011 Dec 15;2(1):29–32.

53. Fahey, F. H. (2002). Data acquisition in PET imaging. Journal of Nuclear Medicine Technology, *30*(2), 39-49

54. Krishnamoorthy S., Schmall J.P., Surti S. 2017. PET physics and instrumentation. In: Khalil M. (eds) Basic Science of PET Imaging. Springer, Cham.

55. Gaertner FC, Fürst S, Schwaiger M. PET/MR: a paradigm shift. Cancer Imaging. 2013 Feb 27;13(1):36–52.

56. Lammertsma AA, Hume SP. Simplified reference tissue model for PET receptor studies. NeuroImage. 1996 Dec;4(3):153–8.

57. Innis RB, Cunningham VJ, Delforge J, Fujita M, Gjedde A, Gunn RN, Holden J, Houle S, Huang SC, Ichise M, Iida H, Ito H, Kimura Y, Koeppe R, Knudsen G, Knuuti J, A Lammertsma A, Laruelle M, Logan J, Maguire RP, Mintun M, Morris E, Parsey R, C Price J, Slifstein M, Sossi V, Suhara T, Votaw J, Wong D , Carson R. Consensus nomenclature for in vivo imaging of reversibly binding radioligands. J Cereb Blood Flow Metab. 2007 Sep 1;27(9):1533–9.

58. Gunn RN, Lammertsma AA, Hume SP, Cunningham VJ. Parametric imaging of ligand-receptor binding in PET Using a simplified reference region model. NeuroImage. 1997 Nov 1;6(4):279–87.

59. Milella, M, Reader A, Albrechtsons D, Minuzzi L, Soucy J, Benkelfat C, Leyton, M, Rosa-Neto P, 2011. Human PET validation study of reference tissue models for the mGluR5 ligand [$_{11}$C]ABP688. Presented at the 41st Annual Meeting of The Society for Neuroscience, Washington, DC.

60. Kokic M, Honer S, M. Ametamey F, Gasparini H, Andres S, Bischoff P. J, Flor M, Heinrich I, Vranesic W, Spooren R, Kuhn P. A, Schubiger. Radiolabelling and in vivo evaluation of 11C-MPEP as a PET radioligand for the imaging of the metabotropic glutamate receptor 5 (MGLUR5). J Label Compd Radiopharm. 2001 May 1;44.

61. Barret O, Tamagnan G, Batis J, Jennings D, Zubal G, Russel D, Marek K, Seiby J. Quantitation of glutamate mGluR5 receptor with 18F-FPEB PET in humans. NeuroImage. 2010 Aug 1;52:S202.

62. Hamill T, Krause S, Ryan C, Bonnefous C, Govek S, Seiders J, Cosford N, Roppe J, Kamenecka J, Patel S, Gibson R, Sanabria S, Riffel K, Eng W, King C, Yang X, Green M, O'Malley S, Burns D. Synthesis, characterization, and first successful monkey imaging studies of metabotropic glutamate receptor subtype 5 (mGluR5) PET radiotracers. Synapse. 2005;56(4):205–16.

63. Ametamey SM, Kessler LJ, Honer M, Wyss MT, Buck A, Hintermann S, Yves P. Auberson, Fabrizio Gasparini, Pius A. Schubiger. Radiosynthesis and preclinical evaluation of 11C-ABP688 as a probe for imaging the metabotropic glutamate receptor subtype 5. J Nucl Med. 2006 Apr 1;47(4):698–705.

64. Treyer V, Streffer J, Ametamey SM, Bettio A, Bläuenstein P, Schmidt M, Gasparini F, Fischer U, Hock C, Buck A. Radiation dosimetry and biodistribution of 11C-ABP688 measured in healthy volunteers. Eur J Nucl Med Mol Imaging. 2008 Apr 1;35(4):766–70.

65. Kawamura K, Yamasaki T, Kumata K, Furutsuka K, Takei M, Wakizaka H, Fujinaga M Kariya K, Yui J, Hatori A, Xie L, Shimoda Y, Hashimoto H, Hayashi K, Zhang M. Binding potential of (E)-[11C]ABP688 to metabotropic glutamate receptor subtype 5 is decreased by the inclusion of its 11C-labelled Z-isomer. Nucl Med Biol. 2014 Jan 1;41(1):17–23.

66. Treyer V, Streffer J, Wyss MT, Bettio A, Ametamey SM, Fischer U, Schmidt M, Gasparini F, Hock C, Buck A. Evaluation of the metabotropic glutamate receptor subtype 5 using PET and 11C-ABP688: Assessment of methods. J Nucl Med. 2007 Jul 1;48(7):1207–15.

67. Smart K, Cox SML, Kostikov A, Shalai A, Scala SG, Tippler M, Jaworska N, Boivin M, Seguin J, Benkelfat C, Leyton M. Effect of (Z)-isomer content on [11C]ABP688 binding potential in humans. Eur J Nucl Med Mol Imaging. 2019 May 1;46(5):1175–8.

68. Bdair H, Tsai I-H, Smart K, Benkelfat C, Leyton M, Kostikov A. Radiosynthesis of the diastereomerically pure (E)-[11 C]ABP688. J Label Compd Radiopharm. 2019;62(12):860–4.

69. Elmenhorst D, Minuzzi L, Aliaga A, Rowley J, Massarweh G, Diksic M, Bauer A, Rosa-Neto P. In vivo and in vitro validation of reference tissue models for the mglur5 ligand [11C]ABP688. J Cereb Blood Flow Metab. 2010 Aug 1;30(8):1538–49.

70. Patel S, Hamill TG, Connolly B, Jagoda E, Li W, Gibson RE. Species differences in mGluR5 binding sites in mammalian central nervous system determined using in vitro binding with [18F]F-PEB. Nucl Med Biol. 2007 Nov 1;34(8):1009–17.

71. DeLorenzo C, Milak MS, Brennan KG, Dileep Kumar JS, Mann JJ, Parsey RV. In vivo positron emission tomography imaging with [11C]ABP688: Binding variability and specificity for the metabotropic glutamate receptor subtype 5 in baboons. Eur J Nucl Med Mol Imaging. 2011 Jun;38(6):1083–94.

72. Wyss MT, Ametamey SM, Treyer V, Bettio A, Blagoev M, Kessler LJ, Burger C, Weber B, Gasparini F, Buck A. Quantitative evaluation of 11C-ABP688 as PET ligand for the measurement of the metabotropic glutamate receptor subtype 5 using autoradiographic studies and a beta-scintillator. NeuroImage. 2007 Apr 15;35(3):1086–92.

73. Akkus F, Terbeck S, Ametamey SM, Rufer M, Treyer V, Burger C, Johayem A, Mancilla BG, Sovago J, Buck A, Hasler G. Metabotropic glutamate receptor 5 binding in patients with obsessive-compulsive disorder. Int J Neuropsychopharmacol. 2014 Dec 1;17(12):1915–22.

74. Milella MS, Marengo L, Larcher K, Fotros A, Dagher A, Rosa-Neto P, Benkelfat, C., Leyton, M. Limbic system mGluR5 availability in cocaine dependent subjects: A high-resolution PET [11C]ABP688 study. NeuroImage. 2014 Sep 1;98:195–202.

75. Akkus F, Treyer V, Johayem A, Ametamey SM, Mancilla BG, Sovago J, Buck A, Hasler, G. (2016). Association of long-term nicotine abstinence with normal metabotropic glutamate Receptor-5 binding. *Biological Psychiatry*, *79*(6), 474–480.

76. Akkus, F, Ametamey, S.M, Treyer, V, Burger C, Johayem, A, Umbricht D, Gomez Mancilla B, Sovago J, Buck A, Hasler G. 2013. Marked global reduction in mGluR5 receptor binding in smokers and ex-smokers determined by [$_{11}$C]ABP688 positron emission tomography. Proc. Natl. Acad. Sci. U. S. A. 110, 737–742.

77. DuBois JM, Rousset OG, Rowley J, Porras-Betancourt M, Reader AJ, Labbe A, Massarweh G, Soucy JP, Rosa-Neto P, Kobayashi E. Characterization of age/sex and the regional distribution of mGluR5 availability in the healthy human brain measured by high-resolution [11C]ABP688 PET. Eur J Nucl Med Mol Imaging. 2016 Jan 1;43(1):152–62.

78. DeLorenzo C, Sovago J, Gardus J, Xu J, Yang J, Behrje R, Kumar JSD, Devanand DP, Pelton GH, Mathis CA, Mason NS, Gomez-Mancilla B, Aizenstein H, Mann JJ, Parsey RV. Characterization of brain mGluR5 binding in a pilot study of late-life major depressive disorder using positron emission tomography and [11C]ABP688. Transl Psychiatry. 2015 Dec;5(12):e693.

79. Miyake N, Skinbjerg M, Easwaramoorthy B, Kumar D, Girgis RR, Xu X, Slifstein M, Abi-Dargham A. Imaging changes in glutamate transmission in vivo with the metabotropic glutamate receptor 5 tracer [11C] ABP688 and N-Acetylcysteine Challenge. Biol Psychiatry. 2011 May 1;69(9):822–4.

80. R Zimmer E, Parent MJ, Leuzy A, Aliaga A, Moquin L, Soucy JP, Skelin I, Gratton A, Gauthier S, Rosa-Neto P. Imaging in vivo glutamate fluctuations with [11C]ABP688: a GLT-1 challenge with ceftriaxone. J Cereb Blood Flow Metab. 2015 Jul;35(7):1169–74.

81. Sandiego CM, Nabulsi N, Lin S-F, Labaree D, Najafzadeh S, Huang Y, Cosgrove K, Carson RE. Studies of the metabotropic glutamate receptor 5 radioligand [11C]ABP688 with N-acetylcysteine challenge in rhesus monkeys. Synapse. 2013;67(8):489–501.

82. DeLorenzo C, Gallezot JD, Gardus J, Yang J, Planeta B, Nabulsi N, R Ogden T, Labaree D, Huang Y, Mann J, Gasparini F, Lin X, Javitch J, Parsey R, Carson R, Esterlis I. In vivo variation in same-day estimates of metabotropic glutamate receptor subtype 5 binding using [11C]ABP688 and [18F]FPEB. J Cereb Blood Flow Metab Off J Int Soc Cereb Blood Flow Metab. 2017 Aug;37(8):2716–27.

83. Prado BM de, Castañeda TR, Galindo A, Arco AD, Segovia G, Reiter RJ. Melatonin disrupts circadian rhythms of glutamate and GABA in the neostriatum of the awake rat: a microdialysis study. J Pineal Res. 2000;29(4):209–16.

84. Elmenhorst D, Mertens K, Kroll T, Oskamp A, Ermert J, Beer S, Coenen HH, Bauer A. Circadian variation of metabotropic glutamate receptor 5 availability in the rat brain. Journal of Sleep Research. 2016 June; 25(6).

85. Laruelle M. Measuring dopamine synaptic transmission with molecular imaging and pharmacological challenges: The State of the Art. In: Gründer G, editor. Molecular Imaging in the Clinical Neurosciences. Totowa, NJ: Humana Press; 2012. p. 163–203.

86. Smart K, Cox SML, Nagano-Saito A, Rosa-Neto P, Leyton M, Benkelfat C. Test–retest variability of [11C]ABP688 estimates of metabotropic glutamate receptor subtype 5 availability in humans. Synapse. 2018 Sep 1;72(9):e22041.

87. Gussew A, Rzanny R, Erdtel M, Scholle HC, Kaiser WA, Mentzel HJ. Time-resolved functional 1H MR spectroscopic detection of glutamate concentration changes in the brain during acute heat pain stimulation. NeuroImage. 2010 Jan 15;49(2):1895–902.

88. Rae CD. A guide to the metabolic pathways and function of metabolites observed in human brain 1H magnetic resonance spectra. Neurochem Res. 2014 Jan 1;39(1):1–36.

89. Bak LK, Schousboe A, Waagepetersen HS. The glutamate/GABA-glutamine cycle: aspects of transport, neurotransmitter homeostasis and ammonia transfer. J Neurochem. 2006;98(3):641–53.

90. Öngür D, Jensen JE, Prescot AP, Stork C, Lundy M, Cohen BM. Abnormal glutamatergic neurotransmission and neuronal-glial interactions in acute mania. Biol Psychiatry. 2008 Oct 15;64(8):718–26.

91. Chiappelli J, Shi Q, Wijtenburg SA, Quiton R, Wisner K, Gaston F. Glutamatergic response to heat pain stress in schizophrenia. Schizophr Bull. 2018 Jun;44(4):886–95.

92. Petroff OA, Mattson RH, Rothman DL. Proton MRS: GABA and glutamate. Adv Neurol. 2000;83:261–71.

93. Govindaraju V, Young K, Maudsley AA. Proton NMR chemical shifts and coupling constants for brain metabolites. NMR Biomed. 2000;13(3):129–53.

94. Ramadan S, Lin A, Stanwell P. Glutamate and glutamine: a review of in vivo MRS in the human brain. NMR Biomed. 2013;26(12):1630–46.

95. Tkác I, Andersen P, Adriany G, Merkle H, Ugurbil K, Gruetter R. In vivo 1H NMR spectroscopy of the human brain at 7 T. Magn Reson Med. 2001 Sep;46(3):451–6.

96. Tkáč I, Gruetter R. Methodology of 1H NMR spectroscopy of the human brain at very high magnetic fields. Appl Magn Reson. 2005 Mar;29(1):139–57.

97. Mullins PG, Chen H, Xu J, Caprihan A, Gasparovic C. Comparative reliability of proton spectroscopy techniques designed to improve detection of J-coupled metabolites. Magn Reson Med. 2008;60(4):964–9.

98. Macrì MA, Garreffa G, Giove F, Guardati M, Ambrosini A, Colonnese C. In vivo quantitative 1H MRS of cerebellum and evaluation of quantitation reproducibility by simulation of different levels of noise and spectral resolution. Magn Reson Imaging. 2004 Dec 1;22(10):1385–93.

99. Dowlati Y, Herrmann N, Swardfager W, Liu H, Sham L, Reim EK, et al. A meta-analysis of cytokines in major depression. Biol Psychiatry. 2010 Mar 1;67(5):446–57.

100. Rosenblat JD, McIntyre RS. Bipolar disorder and inflammation. Psychiatr Clin North Am. 2016 Mar;39(1):125–37.

101. Passos IC, Vasconcelos-Moreno MP, Costa LG, Kunz M, Brietzke E, Quevedo J, F Kapczinski. Inflammatory markers in post-traumatic stress disorder: a systematic review, meta-analysis, and meta-regression. Lancet Psychiatry. 2015 Nov;2(11):1002–12.

102. Tian R, Hou G, Li D, Yuan T-F. A Possible change process of inflammatory cytokines in the prolonged chronic stress and its ultimate implications for health. Sci World J. 2014 June; 780616.

103. Sapolsky R, Rivier C, Yamamoto G, Plotsky P, Vale W. Interleukin-1 stimulates the secretion of hypothalamic corticotropin-releasing factor. Science. 1987 Oct 23;238(4826):522–4.

104. Bekhbat M, Rowson SA, Neigh GN. Checks and balances: the glucocorticoid receptor and nfκb in good times and bad. Front Neuroendocrinol. 2017 Jul;46:15–31.

105. Sorrells SF, Caso JR, Munhoz CD, Sapolsky RM. The Stressed CNS: When glucocorticoids aggravate inflammation. Neuron. 2009 Oct 15;64(1):33–9.

106. Busillo JM, Azzam KM, Cidlowski JA. Glucocorticoids sensitize the innate immune system through regulation of the nlrp3 inflammasome. J Biol Chem. 2011 Nov 4;286(44):38703–13

107. Edwards RR, Kronfli T, Haythornthwaite JA, Smith MT, McGuire L, Page GG. Association of catastrophizing with interleukin-6 responses to acute pain. Pain. 2008 Nov 15;140(1):135–44.

108. Deinzer R, Granrath N, Stuhl H, Twork L, Idel H, Waschul B. Acute stress effects on local Il-1beta responses to pathogens in a human in vivo model. Brain Behav Immun. 2004 Sep;18(5):458–67.

109. Steptoe A, Hamer M, Chida Y. The effects of acute psychological stress on circulating inflammatory factors in humans: a review and meta-analysis. Brain Behav Immun. 2007 Oct;21(7):901–12.

110. Spitzer RL, Williams JB, Gibbon M, First MB. The Structured Clinical Interview for DSM-III-R (SCID). I: History, rationale, and description. Arch Gen Psychiatry. 1992 Aug;49(8):624–9.

111. Pitman RK, Orr SP. Test of the conditioning model of neurosis: differential aversive conditioning of angry and neutral facial expressions in anxiety disorder patients. J Abnorm Psychol. 1986 Aug;95(3):208–13.

112. Davis RC. Modification of the galvanic reflex by daily repetition of a stimulus. J Exp Psychol. 1934;17(4):504–35.

113. Pruessner JC, Kirschbaum C, Meinlschmid G, Hellhammer DH. Two formulas for computation of the area under the curve represent measures of total hormone concentration versus time-dependent change. Psychoneuroendocrinology. 2003 Oct 1;28(7):916–31.

114. Spielberger CD. Manual for the State-Trait Anxiety Inventory STAI (Form Y) ("Self-Evaluation Questionnaire"). 1983 Available from: http://ubir.buffalo.edu/xmlui/handle/10477/1873

115. BIC - The McConnell Brain Imaging Centre: CIVET. Available from: https://www.bic.mni.mcgill.ca/ServicesSoftware/CIVET

116. Fonov V, Evans A, McKinstry R, Almli C, Collins D. Unbiased nonlinear average age-appropriate brain templates from birth to adulthood. NeuroImage. 2009 Jul 1;47:S102.

117. Collins DL, Zijdenbos AP, Baaré WFC, Evans AC. ANIMAL+INSECT: Improved cortical structure segmentation. In: Kuba A, Šáamal M, Todd-Pokropek A, editors. Information Processing in Medical Imaging. Berlin, Heidelberg: Springer; 1999. p. 210–23.

118. Mawlawi O, Martinez D, Slifstein M, Broft A, Chatterjee R, Hwang DR, Huang Y, Simpson N, Ngo K, Van Heertum R, Laruelle M. Imaging human mesolimbic dopamine transmission with positron emission tomography: Accuracy and precision of D2 receptor parameter measurements in ventral striatum. J Cereb Blood Flow Metab 2001 Sep;21(9):1034-57.

119. Abi-Dargham A, Martinez D, Mawlawi O, Simpson N, Hwang D-R, Slifstein M, Anjilvel, Justine Pidcock, Simpson N, Ngo K, Van Heertum R, Laruelle. Measurement of striatal and extrastriatal dopamine d1 receptor binding potential with [11C]NNC112 in humans: Validation and Reproducibility. J Cereb Blood Flow Metab. 2000 Feb 1;20(2):225–43.

120. Kosten L, Verhaeghe J, wyffels L, Stroobants S, Staelens S. Acute ketamine infusion in rat does not affect in vivo [11C]ABP688 binding to metabotropic glutamate receptor subtype 5. Mol Imaging. 2018 Sep 13.17

121. Wyckhuys T, Verhaeghe J, Wyffels L, Langlois X, Schmidt M, Stroobants S, Staelens Sl. N-Acetylcysteine– and MK-801–induced changes in glutamate levels do not affect in vivo binding of metabotropic glutamate 5 receptor radioligand 11C-ABP688 in rat brain. J Nucl Med. 2013 Nov 1;54(11):1954–61.

122. de Kloet ER, Joëls M, Holsboer F. Stress and the brain: from adaptation to disease. Nat Rev Neurosci. 2005 Jun;6(6):463–75.

123. Yuen EY, Liu W, Karatsoreos IN, Ren Y, Feng J, McEwen BS, Yan Z. Mechanisms for acute stress-induced enhancement of glutamatergic transmission and working memory. Mol Psychiatry. 2011 Feb;16(2):156–70.

124. Lupien SJ, Ouellet-Morin I, Hupbach A, Tu MT, Buss C, Walker D. Beyond the stress concept: allostatic load - a developmental biological and cognitive perspective. Developmental Psychopathology; Aprl 2015.14. pp.578-628.

125. Hellhammer DH, Wüst S, Kudielka BM. Salivary cortisol as a biomarker in stress research. Psychoneuroendocrinology. 2009 Feb 1;34(2):163–71.

126. Pruessner JC, Gaab J, Hellhammer DH, Lintz D, Schommer N, Kirschbaum C. Increasing correlations between personality traits and cortisol stress responses obtained by data aggregation. Psychoneuroendocrinology. 1997 Nov;22(8):615–25.

127. Elmenhorst D, Aliaga A, Bauer A, Rosa-Neto P. Test-retest stability of cerebral mGluR5 quantification using [11C]ABP688 and positron emission tomography in rats. Synapse. 2012;66(6):552–60.

128. DeLorenzo C, Kumar JSD, Mann JJ, Parsey RV. In vivo variation in metabotropic glutamate receptor subtype 5 binding using positron emission tomography and [11C]ABP688. J Cereb Blood Flow Metab. 2011 Nov;31(11):2169–80.

129. Hefti K, Holst SC, Sovago J, Bachmann V, Buck A, Ametamey SM, Landolt HP. Increased metabotropic glutamate receptor subtype 5 availability in human brain after one night without sleep. Biol Psychiatry. 2013 Jan 15;73(2):161–8.

130. Hume SP, Opacka-Juffry J, Myers R, Ahier RG, Ashworth S, Brooks DJ, Lammertsma A. Effect of L-dopa and 6-hydroxydopamine lesioning on [11C]raclopride binding in rat striatum, quantified using PET. Synapse. 1995;21(1):45–53.

131. Smart K, Cox SML, Scala SG, Tippler M, Jaworska N, Boivin M, Seguin J, Benkelfat C, Leyton M. Sex differences in [11C]ABP688 binding: A positron emission tomography study of mGlu5 receptors. Eur J Nucl Med Mol Imaging. 2019 May 1;46(5):1179–83.

132. Mathews WB, Kuwabara H, Stansfield K, Valentine H, Alexander M, Kumar A, Gasparini F. Dose-dependent, saturable occupancy of the metabotropic glutamate subtype 5 receptor by fenobam as measured with [11C]ABP688 PET imaging. Synapse. 2014;68(12):565–73.

133. Kågedal M, Cselényi Z, Nyberg S, Raboisson P, Ståhle L, Stenkrona P, Varnäs K, Halldin C, C.Hooker, Karlsson M. A positron emission tomography study in healthy volunteers to estimate mGluR5 receptor occupancy of AZD2066 - Estimating occupancy in the absence of a reference region. NeuroImage. 2013 Nov 15;82:160–9.